

High-order partitioned spectral deferred correction solvers for multiphysics problems

Daniel Z. Huang^a, Will Pazner^b, Per-Olof Persson^c, Matthew J. Zahr^d

^a*Institute for Computational and Mathematical Engineering, Stanford University*

^b*Center for Applied Scientific Computing, Lawrence Livermore National Laboratory*

^c*Department of Mathematics, University of California Berkeley*

^d*Department of Aerospace and Mechanical Engineering, University of Notre Dame*

Abstract

We present an arbitrarily high-order, conditionally stable, partitioned spectral deferred correction (SDC) method for solving multiphysics problems using a sequence of pre-existing single-physics solvers. This method extends the work in [1, 2], which used implicit-explicit Runge-Kutta methods (IMEX) to build high-order, partitioned multiphysics solvers. We consider a generic multiphysics problem modeled as a system of coupled ordinary differential equations (ODEs), coupled through coupling terms that can depend on the state of each subsystem; therefore the method applies to both a semi-discretized system of partial differential equations (PDEs) or problems naturally modeled as coupled systems of ODEs. The sufficient conditions to build arbitrarily high-order partitioned SDC schemes are derived. Based on these conditions, various of partitioned SDC schemes are designed. The stability of the first-order partitioned SDC scheme is analyzed in detail on a coupled, linear model problem. We show that the scheme is conditionally stable, and under conditions on the coupling strength, the scheme can be unconditionally stable. We demonstrate the performance of the proposed partitioned solvers on several classes of multiphysics problems with moderate coupling strength. They include a stiff linear system of ODEs, advection-diffusion-reaction systems, and fluid-structure interaction problems with both incompressible and compressible flows, where we verify the design order of the SDC schemes and study various stability properties. We also directly compare the accuracy, stability, and cost of the proposed partitioned SDC solver with the partitioned IMEX method in [1, 2] on this suite of test problems. The results suggest that the high-order partitioned SDC solvers are more robust than the partitioned IMEX solvers for the numerical examples considered in this work, while the IMEX methods require fewer implicit solves.

1. Introduction

The numerical simulation of multiphysics problems involving multiple physical models or multiple simultaneous physical phenomena is significant in many engineering and scientific applications, e.g., fluid-structure interactions (FSI) in aeroelasticity [3, 4, 5] or biomechanics [6, 7, 8], chemical reaction in combustion or subsurface flows [9, 10], electricity and magnetism with hydrodynamics in plasma physics [11, 12, 13], among others. These problems are generally highly nonlinear, feature multiple scales and strong coupling effects, and require heterogeneous discretizations for the various physics subsystems. To balance the treatment of these features, solution strategies ranging from monolithic approaches to partitioned procedures have been proposed.

In the monolithic approach [14, 15, 16], all physical subsystems are solved simultaneously. Therefore, this approach is preferred in the case of strong interactions to ensure stability. However, when the coupled subsystems are complex, the monolithic procedure often requires significant implementation effort since only small components of existing software can be re-used. An alternative is the partitioned procedure [17, 18, 19], also known as a staggered or a loosely coupled procedure, where different subsystems are modeled and discretized separately, and the resulting equations are solved independently. The coupling occurs through specific terms that are lagged to previous time instances and communicated between solvers. This procedure facilitates software modularity and mathematical modeling; however, these schemes are often low-order accurate [18] and may suffer from lack of stability [20].

Email addresses: zhengyuh@stanford.edu (Daniel Z. Huang), pazner1@llnl.gov (Will Pazner), persson@berkeley.edu (Per-Olof Persson), mzahr@nd.edu (Matthew J. Zahr)

Recently, a partitioned solver based on implicit-explicit Runge-Kutta schemes, first proposed to solve stiff additive ordinary differential equations [21, 22], was proposed [23, 24] in the context of a specific multiphysics system: fluid-structure interaction. This idea is generalized in [1] to build a framework to construct high-order, partitioned solvers based on monolithic IMEX discretizations for general multiphysics systems. Specific implicit-explicit decompositions and consistent predictors are designed to allow the monolithic discretization to be solved in a partitioned manner, i.e., subsystem-by-subsystem, and meanwhile, maintain arbitrarily high-order accuracy and reasonable stability properties. However, due to the explicit component in the IMEX schemes, these partitioned solvers cannot handle differential-algebraic systems, due to the singular mass matrix.

This work extends the work in [1], and presents arbitrarily high-order *partitioned* spectral deferred correction schemes for general multiphysics systems. The SDC method, first proposed in [25], is a general class of methods for solving initial value problems determined by ordinary differential equations (ODEs), wherein high-order accuracy is attained by performing a series of correction sweeps using a low-order time-stepping method. Implicit versions of this method are shown to have good stability even for stiff equations [26, 27, 28]. One of the most attractive features of SDC is the flexibility in the choice of the low order solver for the correction equation. As for multiphysics systems, when a partitioned low-order solver is chosen, the proposed multiphysics solver can be both arbitrarily high-order accurate and partitioned. In the present work, these low-order partitioned solvers are designed using the weakly coupled Gauss-Seidel predictor proposed in [1], which features good stability. The accuracy and stability properties of these partitioned multiphysics solvers are analyzed both analytically and numerically. The comparisons with the partitioned IMEX method in [1] are presented, which suggest the high-order partitioned SDC solvers are more robust than the partitioned IMEX solvers, while the IMEX are more efficient for the numerical examples considered in this work. Moreover, it is worth mentioning, the present SDC scheme is capable of handling differential-algebraic systems of equations (DAE), which is demonstrated in section 5.3.

The remainder of the paper is organized as follows. In Section 2, the general form of the multiphysics problem as a system of m systems of partial differential equations and its semi-discretization are introduced. In Section 3, an overview of SDC schemes is provided. In Section 4, the arbitrarily high-order SDC solvers are introduced and their features such as accuracy and stability are discussed. Numerical applications are provided in Section 5 that demonstrate the high-order accuracy and good stability properties of the proposed solvers on an ODE system, an advection-diffusion-reaction system, and fluid-structure interaction problems with both incompressible flows and compressible flows.

2. Governing multiphysics equations and semi-discrete formulation

As in the works [1, 2], we consider a general formulation for multiple interacting physical processes, described by a coupled system of partial differential equations,

$$\frac{\partial u^i}{\partial t} = \mathcal{L}^i(u^i, \mathbf{c}^i, \mathbf{x}, t), \quad \mathbf{x} \in \Omega^i(\mathbf{c}^i), \quad t \in [0, T], \quad (1)$$

for $1 \leq i \leq m$, where m denotes the number of physical subsystems. Appropriate boundary conditions, omitted here for brevity, are enforced for each of the subsystems. The i th physical subsystem is modeled as a partial differential equation with corresponding differential operator denoted as \mathcal{L}^i . The state variable $u^i(\mathbf{x}, t)$ denotes the solution to the i th equation in the spatial domain Ω^i , in the time interval $[0, T]$. The coupling between the physical subsystems is described through the *coupling term* $\mathbf{c}^i(u^1, \dots, u^m, \mathbf{x}, t)$, which couples the i th subsystem to the $m - 1$ remaining subsystems. In the most general case, the differential operator \mathcal{L}^i , spatial domain Ω^i , and boundary conditions all depend on this coupling term.

In this work, we are concerned with the temporal integration of the coupled system eq. (1). We first begin by assuming a spatial discretization for each of the physical subsystems, and then writing a general semi-discretized form for the i th subsystem as a system of ordinary differential equations

$$\mathbf{M}^i \frac{\partial \mathbf{u}^i}{\partial t} = \mathbf{r}^i(\mathbf{u}^i, \mathbf{c}^i, t), \quad t \in [0, T], \quad (2)$$

where \mathbf{M}^i denotes the fixed mass matrix and \mathbf{r}^i denotes the spatial residual corresponding to a spatial discretization of the problem. Here we use the notation \mathbf{u}^i to denote the discretized solution represented as a vector of degrees

of freedom. In general, the coupling term \mathbf{c}^i will result in a coupling between all m subsystems of ODEs given by eq. (2). We can write this large, coupled system of equations in the simple form as

$$\mathbf{M} \frac{\partial \mathbf{u}}{\partial t} = \mathbf{r}(\mathbf{u}, \mathbf{c}, t), \quad t \in [0, T], \quad (3)$$

where \mathbf{u} , \mathbf{c} , and \mathbf{r} represent the state vectors, coupling terms, and spatial residuals for each of the single-physics subsystems concatenated as

$$\mathbf{u} = \begin{pmatrix} \mathbf{u}^1 \\ \vdots \\ \mathbf{u}^m \end{pmatrix}, \quad \mathbf{c} = \begin{pmatrix} \mathbf{c}^1 \\ \vdots \\ \mathbf{c}^m \end{pmatrix}, \quad \mathbf{r} = \begin{pmatrix} \mathbf{r}^1(\mathbf{u}^1, \mathbf{c}^1, t) \\ \vdots \\ \mathbf{r}^m(\mathbf{u}^m, \mathbf{c}^m, t) \end{pmatrix}. \quad (4)$$

The mass matrix \mathbf{M} is considered to be a block-diagonal matrix with the single-physics mass matrices \mathbf{M}^i along the diagonal,

$$\mathbf{M} = \begin{pmatrix} \mathbf{M}^1 & & \\ & \ddots & \\ & & \mathbf{M}^m \end{pmatrix}. \quad (5)$$

In order to construct *partitioned* time integration schemes for the system eq. (3), we write the total derivative of the spatial residuals \mathbf{r} as

$$D_{\mathbf{u}} \mathbf{r} = \frac{\partial \mathbf{r}}{\partial \mathbf{u}} + \frac{\partial \mathbf{r}}{\partial \mathbf{c}} \frac{\partial \mathbf{c}}{\partial \mathbf{u}}. \quad (6)$$

The terms on the right-hand side of this equation are Jacobian matrices with block structures given by

$$\frac{\partial \mathbf{r}}{\partial \mathbf{u}} = \begin{pmatrix} \frac{\partial \mathbf{r}^1}{\partial \mathbf{u}^1} & & \\ & \ddots & \\ & & \frac{\partial \mathbf{r}^m}{\partial \mathbf{u}^m} \end{pmatrix}, \quad \frac{\partial \mathbf{r}}{\partial \mathbf{c}} = \begin{pmatrix} \frac{\partial \mathbf{r}^1}{\partial \mathbf{c}^1} & & \\ & \ddots & \\ & & \frac{\partial \mathbf{r}^m}{\partial \mathbf{c}^m} \end{pmatrix}, \quad \frac{\partial \mathbf{c}}{\partial \mathbf{u}} = \begin{pmatrix} \frac{\partial \mathbf{c}^1}{\partial \mathbf{u}^1} & \cdots & \frac{\partial \mathbf{c}^1}{\partial \mathbf{u}^m} \\ \vdots & \ddots & \vdots \\ \frac{\partial \mathbf{c}^m}{\partial \mathbf{u}^1} & \cdots & \frac{\partial \mathbf{c}^m}{\partial \mathbf{u}^m} \end{pmatrix}. \quad (7)$$

The term $\frac{\partial \mathbf{r}}{\partial \mathbf{u}}$ is block diagonal, and represents the contribution of a given physics state to its own subsystem. The second term, $\frac{\partial \mathbf{r}}{\partial \mathbf{c}} \frac{\partial \mathbf{c}}{\partial \mathbf{u}}$ represents the coupling between subsystems.

Remark 1. *The coupled system of ODEs in (2) or (3) is the starting point for the mathematical formulation of the proposed high-order, partitioned SDC method; therefore the method applied to problems directly modeled as a system of ODEs in addition to ODEs that result from semi-discretization of a system of PDEs.*

3. Spectral Deferred Corrections

Spectral deferred correction methods are a class of numerical methods for approximating the solution to ordinary differential equations through an iterative process based on the Picard equation [25]. These methods have garnered a large amount of interest [26, 28, 29], and have been applied to a wide variety of problems [27, 30, 31, 32, 33]. An attractive feature of SDC methods is that they are capable of arbitrary formal order of accuracy. Additionally, their implementation is relatively straightforward, since they are typically built by combining simple low-order methods, such as forward Euler or backward Euler. Additionally, and most importantly for this work, the iterative nature of SDC methods is very flexible, allowing for sophisticated semi- and multi-implicit splitting schemes [26, 27, 33]. It is this flexibility that will allow us to construct efficient partitioned multiphysics integrators.

We begin by considering an ordinary differential equation given by

$$\frac{d\mathbf{u}(t)}{dt} = \mathbf{r}(\mathbf{u}, t), \quad (8)$$

with initial condition $\mathbf{u}(t_n) = \mathbf{u}_n$. The SDC method is a one-step method to advance the solution from t_n to $t_{n+1} = t_n + \Delta t$. Integrating from t_n to t (for arbitrary $t > t^n$), we obtain the associated integral equation,

$$\mathbf{u}(t) = \mathbf{u}_n + \int_{t_n}^t \mathbf{r}(\mathbf{u}(\tau), \tau) d\tau. \quad (9)$$

For the sake of brevity, we will omit the dependence of \mathbf{r} on t . As the SDC method is an iterative process, let k denote the iterative index and $\mathbf{u}^{(k)}(t)$ denote an approximation to the solution $\mathbf{u}(t)$ of the k th iterate. The SDC method seeks to obtain an improved approximation $\mathbf{u}^{(k+1)}(t)$ by approximating the solution to the correction equation

$$\mathbf{u}^{(k+1)}(t) = \mathbf{u}_n + \int_{t_n}^t \left(\mathbf{r}(\mathbf{u}^{(k+1)}) - \mathbf{r}(\mathbf{u}^{(k)}) \right) d\tau + \int_{t_n}^t \mathbf{r}(\mathbf{u}^{(k)}) d\tau. \quad (10)$$

In order to obtain the SDC method, this correction equation is discretized by replacing the integrals with approximations computed using quadrature rules. The first integral on the right-hand side of eq. (10) is discretized using a low-order method (with order of accuracy p_{low} , typically $p_{\text{low}} = 1$). This low-order method usually corresponds to forward or backward Euler. The second integral is approximated using a high-order quadrature rule with order of accuracy p_{high} . Each iteration updates the solution from $\mathbf{u}^{(k)}$ to $\mathbf{u}^{(k+1)}$, improving the order of accuracy of the provision solution by p_{low} , up to a maximum of p_{high} [25].

We begin by selecting a high-order accurate quadrature rule on the interval $[t^n, t^n + \Delta t]$. The order of accuracy of this quadrature rule, denoted p_{high} , is equal to the formal order of accuracy of the resulting SDC method. The abscissas of this quadrature rule, which we denote

$$t_n = t_{n,0} < t_{n,1} < \dots < t_{n,q} = t_n + \Delta t, \quad (11)$$

can be considered to be nodes at which we approximate the solution to the ODE. For simplicity of notation, we have included the left and right endpoints of the interval as points in the quadrature rule. This choice is made for uniformity of notation, and more general quadrature rules can be considered by assigning zero quadrature weights to one or both of the endpoints. The temporal nodes eq. (11) give rise to q time sub-steps $[t_{n,j}, t_{n,j+1}]$ for $0 \leq j \leq q-1$, with $\Delta t_{n,j} = t_{n,j+1} - t_{n,j}$. Given a function whose value is known at each of the temporal nodes, its integral over the sub-interval can be approximated by integrating the resulting interpolating polynomial. Thus, given a function $\psi(t)$ and nodal values $\psi_i = \psi(t_{n,i})$, we introduce the notation $I_j^{j+1}\psi$ to denote the resulting approximation to $\int_{t_{n,j}}^{t_{n,j+1}} \psi(\tau) d\tau$,

$$I_j^{j+1}\psi = \int_{t_{n,j}}^{t_{n,j+1}} \psi(\tau) d\tau = \sum_{i=0}^q w_i^j \psi_i, \quad (12)$$

here w_i^j is the weight related to abscissa $t_{n,i}$.

Given a previous approximation $\mathbf{u}_{n,j}^{(k)}$ for $0 \leq j \leq q$ at the k th iteration and a current approximation $\mathbf{u}_{n,j}^{(k+1)}$, the SDC method produces an updated approximation at the next temporal node $\mathbf{u}_{n,j+1}^{(k+1)}$ by discretizing eq. (10). In particular, if forward Euler is used for the low-order quadrature rule, the solution at the next temporal node is given by the following *explicit* update:

$$\text{Forward Euler:} \quad \mathbf{u}_{n,j+1}^{(k+1)} = \mathbf{u}_{n,j}^{(k+1)} + \Delta t_{n,j} \left(\mathbf{r}(\mathbf{u}_{n,j}^{(k+1)}) - \mathbf{r}(\mathbf{u}_{n,j}^{(k)}) \right) + I_j^{j+1} \mathbf{r}(\mathbf{u}_n^{(k)}). \quad (13)$$

Similarly, if backward Euler is used for the low-order quadrature, the solution at the next temporal node is given by the following *implicit* update:

$$\text{Backward Euler:} \quad \mathbf{u}_{n,j+1}^{(k+1)} = \mathbf{u}_{n,j}^{(k+1)} + \Delta t_{n,j} \left(\mathbf{r}(\mathbf{u}_{n,j+1}^{(k+1)}) - \mathbf{r}(\mathbf{u}_{n,j+1}^{(k)}) \right) + I_j^{j+1} \mathbf{r}(\mathbf{u}_n^{(k)}). \quad (14)$$

Thus, given approximations $\mathbf{u}_{n,j}^{(k)}$ for $0 \leq j \leq q$, improved approximations $\mathbf{u}_{n,j}^{(k+1)}$ are obtained through a sequence of forward or backward Euler steps. Each update from $\mathbf{u}_n^{(k)}$ to $\mathbf{u}_n^{(k+1)}$, termed an *SDC sweep*, increases the order of accuracy of the solution by p_{low} , up to a maximum order of p_{high} . Therefore, when using backward or forward Euler corrections, p_{high} iterations are generally required to achieve a formal order accuracy of p_{high} . Starting this process requires an initial guess for the solution $\mathbf{u}_{n,j}^{(0)}$ for $0 \leq j \leq q$. Typically it is sufficient to use the previous step solution $\mathbf{u}_{n,j}^{(0)} = \mathbf{u}_n$ as an initial guess.

It can be useful to note that the SDC iterations can be viewed as a fixed-point iteration, converging to the collocation solution $\mathbf{u}_j^{\text{col}}$, which satisfies

$$\mathbf{u}_{n,j+1}^{\text{col}} = \mathbf{u}_{n,j}^{\text{col}} + I_j^{j+1} \mathbf{r}(\mathbf{u}_n^{\text{col}}). \quad (15)$$

Collocation schemes have been studied extensively in the context of fully-implicit Runge-Kutta methods [34, 35, 29]. These methods typically have very attractive stability and accuracy properties; however, solving the resulting algebraic systems may be challenging.

4. Partitioned SDC schemes for multiphysics

In this work, we consider implicit SDC methods corresponding to the discretized system eq. (14). A straightforward application of this scheme to the multiphysics system eq. (3) results in

$$M^i \mathbf{u}_{n,j+1}^{i,(k+1)} = M^i \mathbf{u}_{n,j}^{i,(k+1)} + \Delta t_{n,j} \left(\mathbf{r}^i(\mathbf{u}_{n,j+1}^{i,(k+1)}, \mathbf{c}_{n,j+1}^{i,(k+1)}) - \mathbf{r}^i(\mathbf{u}_{n,j+1}^{i,(k)}, \mathbf{c}_{n,j+1}^{i,(k)}) \right) + I_j^{j+1} \mathbf{r}(\mathbf{u}_n^{i,(k)}, \mathbf{c}_n^{i,(k)}). \quad (16)$$

Here the first superscript i represents the subsystem number, the second superscript k represents the iteration number, and the subscript n and j represent the time step and the abscissa. The main challenge in solving the resulting system of equations is the coupling term $\mathbf{c}_{n,j+1}^{i,(k+1)}$, which, in general, results in a fully-coupled system of equations. In order to reduce this coupling, we introduce certain approximations to this coupling term based on the predictors introduced in [1]. The main idea of the present approach is to reduce the coupling by making use of the state variables from the previous *iterate* when evaluating the coupling term. This is in contrast to the IMEX methods presented in [1], which lagged the coupling terms one time step to maintain the design order of the IMEX scheme. We consider only the weak Gauss-Seidel type predictor $\tilde{\mathbf{c}}_{n,j+1}^{i,(k+1)}$ for the i th subsystem, defined as follows:

$$\tilde{\mathbf{c}}_{n,j+1}^{i,(k+1)} = \mathbf{c}(\mathbf{u}_{n,j+1}^{1,(k+1)}, \dots, \mathbf{u}_{n,j+1}^{i-1,(k+1)}, \mathbf{u}_{n,j+1}^{i,(k)}, \dots, \mathbf{u}_{n,j+1}^m(k)), \quad (17)$$

which depends on the the most up-to-date information from the previous $i - 1$ subsystems. This choice of predictor implies the *ordering* of the subsystems is important; see [1] for a general discussion of the ordering of subsystems in the context of Gauss-Seidel predictors for multiphysics partitioned solvers and Section 5 for the ordering used for the applications considered in this work.

This choice of predictor is quite simple to implement, and its robustness has been demonstrated in [1]. The partitioned solver is then constructed by replacing the term $\mathbf{c}_{n,j+1}^{i,(k+1)}$ in eq. (16) with its appropriately chosen approximation $\tilde{\mathbf{c}}_{n,j+1}^{i,(k+1)}$. The detailed algorithm is summarized in Algorithm 1. It is also worth mentioning that to solve the system eq. (16) for $\mathbf{u}_{n,j+1}^{i,(k+1)}$ with the approximation eq. (17), only the single-physics Jacobian $\frac{\partial \mathbf{r}^i}{\partial \mathbf{u}^i}$ is required because $\tilde{\mathbf{c}}_{n,j+1}^{i,(k+1)}$ does not depend on $\mathbf{u}_{n,j+1}^{i,(k+1)}$.

Algorithm 1 Spectral deferred correction partitioned multiphysics scheme

- 1: Set 0th sweep values $\mathbf{u}_{n,j}^{i,(0)} = \mathbf{u}_n^i$ for $i = 1, \dots, m, j = 0, \dots, q$
- 2: **for** iterations $k = 0, \dots, p_{\text{high}} - 1$ **do**
- 3: Set $\mathbf{u}_{n,0}^{i,(k)} = \mathbf{u}_n^i$ for $i = 1, \dots, m$
- 4: **for** abscissas $j = 0, \dots, q - 1$ **do**
- 5: **for** physical subsystems $i = 1, \dots, m$ **do**
- 6: Implicit solve for $\mathbf{u}_{n,j+1}^{i,(k+1)}$:

$$M^i \mathbf{u}_{n,j+1}^{i,(k+1)} = M^i \mathbf{u}_{n,j}^{i,(k+1)} + \Delta t_{n,j} \left(\mathbf{r}^i(\mathbf{u}_{n,j+1}^{i,(k+1)}, \tilde{\mathbf{c}}_{n,j+1}^{i,(k+1)}) - \mathbf{r}^i(\mathbf{u}_{n,j+1}^{i,(k)}, \mathbf{c}_{n,j+1}^{i,(k)}) \right) + I_j^{j+1} \mathbf{r}(\mathbf{u}_n^{i,(k)}, \mathbf{c}_n^{i,(k)})$$

- 7: **end for**
 - 8: **end for**
 - 9: **end for**
 - 10: Set $\mathbf{u}_{n+1}^i = \mathbf{u}_{n,q}^{i,p_{\text{high}}}$ for $i = 1, \dots, m$
-

4.1. Partitioned SDC schemes

Based on the discussion above, we build a family of partitioned SDC schemes by choosing different quadrature points for algorithm 1, which are listed as follows

1. The first-order scheme ($p_{\text{high}} = 1$), with 2 abscissas $\{0, 1\}$. The corresponding integrals in eq. (12) are defined as

$$I_0^1 \psi = \Delta t \psi(1),$$

which is abbreviated as SDC1.

2. The second-order scheme ($p_{high} = 2$), with 2 abscissas $\{0, 1\}$. The corresponding integrals in eq. (12) are defined as

$$I_0^1 \psi = \frac{\Delta t}{2} \psi(0) + \frac{\Delta t}{2} \psi(1),$$

which is abbreviated as SDC2.

3. The third-order scheme ($p_{high} = 3$), with 3 Gauss-Radau abscissas $\{0, \frac{1}{3}, 1\}$. The corresponding integrals in eq. (12) are defined as

$$I_0^1 \psi = \frac{5\Delta t}{12} \psi\left(\frac{1}{3}\right) - \frac{\Delta t}{12} \psi(1) \quad \text{and} \quad I_1^2 \psi = \frac{\Delta t}{3} \psi\left(\frac{1}{3}\right) + \frac{\Delta t}{3} \psi(1),$$

which is abbreviated as SDC3-r, for this case, the lower order approximation is specifically chosen (see remark 3) as

$$\mathcal{C}_j = \Delta t \left(\mathbf{r}^i(\mathbf{u}_{n,j+1}^{i,(k+1)}, \tilde{\mathbf{c}}_{n,j+1}^{i,(k+1)}) - \mathbf{r}^i(\mathbf{u}_{n,j+1}^{i,(k)}, \mathbf{c}_{n,j+1}^{i,(k)}) \right),$$

where Δt is used instead of $\Delta t_{n,j}$.

4. The third-order scheme ($p_{high} = 4$), with 3 Gauss-Lobatto abscissas $\{0, \frac{1}{2}, 1\}$. The corresponding integrals in eq. (12) are defined as

$$I_0^1 \psi = \frac{5\Delta t}{24} \psi(0) + \frac{8\Delta t}{24} \psi\left(\frac{1}{2}\right) - \frac{\Delta t}{24} \psi(1) \quad \text{and} \quad I_1^2 = -\frac{\Delta t}{24} \psi(0) + \frac{8\Delta t}{24} \psi\left(\frac{1}{2}\right) + \frac{5\Delta t}{24} \psi(1),$$

which is abbreviated as SDC3-l. This scheme uses a fourth-order quadrature, but only three SDC sweeps.

5. The fourth-order scheme ($p_{high} = 4$), with 3 Gauss-Lobatto abscissas $\{0, \frac{1}{2}, 1\}$. The corresponding integrals in eq. (12) are defined as

$$I_0^1 \psi = \frac{5\Delta t}{24} \psi(0) + \frac{8\Delta t}{24} \psi\left(\frac{1}{2}\right) - \frac{\Delta t}{24} \psi(1) \quad \text{and} \quad I_1^2 = -\frac{\Delta t}{24} \psi(0) + \frac{8\Delta t}{24} \psi\left(\frac{1}{2}\right) + \frac{5\Delta t}{24} \psi(1),$$

which is abbreviated as SDC4.

4.2. Accuracy of the partitioned SDC schemes

To analyze the order of accuracy of our partitioned SDC schemes, let $\mathbf{u}(t)$ be the exact solution of eq. (8), which satisfies

$$\mathbf{u}(t_{n,j+1}) = \mathbf{u}(t_{n,j}) + \int_{t_{n,j}}^{t_{n,j+1}} \mathbf{r}(\mathbf{u}(\tau), \tau) d\tau, \quad (18)$$

here we assume the function \mathbf{r} is C^1 continuous, which is sufficient to guarantee the local existence and uniqueness of the solution. Let L denote the Lipschitz constant of \mathbf{r} .

The update equations (eq. (13), eq. (14), or line 6 in algorithm 1) are written in a general form as

$$\mathbf{u}_{n,j+1}^{(k+1)} = \mathbf{u}_{n,j}^{(k+1)} + \mathcal{C}_j(\mathbf{u}_n^{(k+1)}, \mathbf{u}_n^{(k)}) + I_j^{j+1} \mathbf{r}(\mathbf{u}_n^{(k)}), \quad (19)$$

where $\mathcal{C}_j(\mathbf{u}_n^{(k+1)}, \mathbf{u}_n^{(k)})$ denotes the low-order approximation from $t_{n,j}$ to $t_{n,j+1}$. We now give the *local error* of SDC schemes by induction, on the assumption that the numerical solution at the previous solution point t_n is exact. This result extends standard convergence results in the SDC literature [36, 29, 37] to the case of the partitioned SDC presented here.

Theorem 1. *We assume that the low-order correction $\mathcal{C}_j(\cdot, \cdot)$ satisfies the following Lipschitz-type conditions:*

$$\begin{aligned} \left\| \mathcal{C}_j(\mathbf{u}_n^{(k+1)}, \mathbf{u}_n^{(k)}) - \mathcal{C}_j(\mathbf{u}(t_{n,j}), \mathbf{u}_n^{(k)}) \right\| &\leq C \Delta t L \sum_{j' \leq j+1} \|\mathbf{u}_{n,j'}^{(k+1)} - \mathbf{u}(t_{n,j'})\|, \\ \left\| \mathcal{C}_j(\mathbf{u}(t_{n,j}), \mathbf{u}_n^{(k)}) \right\| &\leq C \Delta t L \sum_{j' \leq j+1} \|\mathbf{u}(t_{n,j'}) - \mathbf{u}_{n,j'}^{(k)}\|, \end{aligned} \quad (20)$$

where the constant C is independent of j , k , and Δt . Then, we have the following estimate for the local error of the SDC scheme:

$$\|\mathbf{u}_{n,j}^{(k)} - \mathbf{u}(t_{n,j})\| = \mathcal{O}\left(\Delta t^{\min\{k+1, p_{high}+1\}}\right) \quad \text{for } 0 \leq j \leq q, 0 \leq k. \quad (21)$$

Proof. We proceed by induction on j and k . It is easy to verify that eq. (21) holds for base cases with $j = 0$ or $k = 0$. Subtracting eq. (18) from eq. (19), we have

$$\mathbf{u}_{n,j+1}^{(k+1)} - \mathbf{u}(t_{n,j+1}) = \mathbf{u}_{n,j}^{(k+1)} - \mathbf{u}(t_{n,j}) + \mathcal{C}_j(\mathbf{u}_n^{(k+1)}, \mathbf{u}_n^{(k)}) + I_j^{j+1} \mathbf{r}(\mathbf{u}_n^{(k)}) - \int_{t_{n,j}}^{t_{n,j+1}} \mathbf{r}(\mathbf{u}(\tau)) d\tau. \quad (22)$$

Since the underlying quadrature rule has order of accuracy p_{high} , we have

$$I_j^{j+1} \mathbf{r}(\mathbf{u}_n^{(k)}) - \int_{t_{n,j}}^{t_{n,j+1}} \mathbf{r}(\mathbf{u}(\tau)) d\tau = I_j^{j+1} [\mathbf{r}(\mathbf{u}_n^{(k)}) - \mathbf{r}(\mathbf{u}(t))] + \Delta t_{n,j} \mathcal{O}(\Delta t^{p_{high}}). \quad (23)$$

By induction, we assume eq. (21) holds for all $k' \leq k$ and $k' = k + 1, j' \leq j$. Using the inductive assumption, we have

$$\mathbf{u}_{n,j}^{(k+1)} - \mathbf{u}(t_{n,j}) = \mathcal{O}(\Delta t^{\min\{k+2, p_{high}+1\}}). \quad (24)$$

Making use of eq. (23) and eq. (24), we see that eq. (22) is then reduced to

$$\mathbf{u}_{n,j+1}^{(k+1)} - \mathbf{u}(t_{n,j+1}) = \mathcal{C}_j(\mathbf{u}_n^{(k+1)}, \mathbf{u}_n^{(k)}) + \mathcal{O}(\Delta t^{\min\{k+2, p_{high}+1\}}). \quad (25)$$

By using property (20) and induction on k , we have

$$\begin{aligned} \|\mathcal{C}_j(\mathbf{u}_n^{(k+1)}, \mathbf{u}_n^{(k)})\| &= \|\mathcal{C}_j(\mathbf{u}_n^{(k+1)}, \mathbf{u}_n^{(k)}) - \mathcal{C}_j(\mathbf{u}, \mathbf{u}_n^{(k)}) + \mathcal{C}_j(\mathbf{u}, \mathbf{u}_n^{(k)})\| \\ &\leq \sum_{j' \leq j+1} C \Delta t L \|\mathbf{u}_{n,j'}^{(k+1)} - \mathbf{u}(t_{n,j'})\| + \Delta t \mathcal{O}(\Delta t^{\min\{k+1, p_{high}+1\}}), \end{aligned}$$

Now, by induction on j , we obtain

$$(1 - C \Delta t L) \|\mathbf{u}_{n,j+1}^{(k+1)} - \mathbf{u}(t_{n,j+1})\| = \sum_{j' \leq j} C \Delta t L \|\mathbf{u}_{n,j'}^{(k+1)} - \mathbf{u}(t_{n,j'})\| + \mathcal{O}(\Delta t^{\min\{k+2, p_{high}+1\}}) = \mathcal{O}(\Delta t^{\min\{k+2, p_{high}+1\}}).$$

Therefore, eq. (21) holds for all $k \geq 0$ and $0 \leq j \leq q$. This finishes our proof of eq. (21), which also indicates the optimal global error of SDC schemes is $\mathcal{O}(\Delta t^{p_{high}})$, when p_{high} sweeps are applied. \square

Remark 2. As for the hypothesis (20) of Theorem 1, it is easy to verify that the forward Euler approximation eq. (13), backward Euler approximation eq. (14) and our weak Gauss-Seidel predictor based approximation in algorithm 1 all satisfy the sufficient conditions. Therefore, these three approximations can all lead to design order of accuracy.

Remark 3. For these three schemes, even if we change $\Delta t_{n,j}$ to $\alpha_j \Delta t_{n,j}$ (See SDC3-r), for any $\alpha_j = \mathcal{O}(1)$ in the low order approximation \mathcal{C}_j , the sufficient condition (20) still holds. That means to achieve arbitrary high order accuracy, the low order approximation \mathcal{C}_j in SDC schemes is not required to be an accurate approximation, which gives more flexibility to design new stable schemes.

4.3. Stability of the partitioned SDC schemes

The stability properties of SDC schemes have been *numerically* analyzed widely in [25, 27, 29], in which L-stable and A-stable properties are reported. We will analyze the stability of the partitioned SDC schemes based on a model linear system

$$\dot{\mathbf{u}} = \mathbf{A} \mathbf{u} \quad (26)$$

where $\mathbf{A} = \mathbf{L} + \mathbf{D} + \mathbf{U}$ is an $n \times n$ matrix, \mathbf{L} is the lower triangular part of \mathbf{A} , \mathbf{U} is the upper triangular part of \mathbf{A} , and \mathbf{D} is the diagonal of \mathbf{A} . The system is treated as n subsystems and the coupling term is taken as $\mathbf{c}(\mathbf{u}) = (\mathbf{L} + \mathbf{U})\mathbf{u}$. We will prove SDC1 scheme is unconditionally stable, when \mathbf{A} is strictly diagonally dominant with non-positive diagonal entries. The update matrix for the SDC1 takes the form

$$\mathbf{C} = (\mathbf{I} - \Delta t \mathbf{L} - \Delta t \mathbf{D})^{-1} (\mathbf{I} + \Delta t \mathbf{U}). \quad (27)$$

Any of its eigenpairs (λ, \mathbf{x}) with $|\lambda| \geq 1$ satisfy the relation

$$(\mathbf{I} - \Delta t \mathbf{L} - \Delta t \mathbf{D})^{-1}(\mathbf{I} + \Delta t \mathbf{U})\mathbf{x} = \lambda \mathbf{x}, \quad (28)$$

which can be re-arranged as

$$(\mathbf{I} + \Delta t \mathbf{U})\mathbf{x} = (\mathbf{I} - \Delta t \mathbf{L} - \Delta t \mathbf{D})\lambda \mathbf{x} \quad (29)$$

or written as components as

$$x_i + \Delta t \sum_{j>i} a_{ij} x_j + \Delta t \lambda \sum_{j<i} a_{ij} x_j = \lambda x_i - \Delta t \lambda a_{ii} x_i \quad (30)$$

for $i = 1, \dots, N$. Application of the triangular inequality and division by $|x_i|$ leads to the relation

$$1 + \Delta t \sum_{j>i} |a_{ij}| \frac{|x_j|}{|x_i|} + \Delta t |\lambda| \sum_{j<i} |a_{ij}| \frac{|x_j|}{|x_i|} \geq |\lambda| |1 - \Delta t a_{ii}|. \quad (31)$$

The assumption of strictly diagonal dominance and negative diagonal entries leads to the following bound

$$|\lambda| |1 - \Delta t a_{ii}| = |\lambda| (1 + \Delta t |a_{ii}|) > |\lambda| (1 + \Delta t \sum_{j \neq i} |a_{ij}|). \quad (32)$$

On the other hand, if $i = \arg \max_{1 \leq j \leq n} |x_j|$, (31) leads to

$$1 + \Delta t \sum_{j>i} |a_{ij}| + \Delta t |\lambda| \sum_{j<i} |a_{ij}| \geq |\lambda| |1 - \Delta t a_{ii}|. \quad (33)$$

Combining (32) and (33), we arrive at

$$1 + \Delta t \sum_{j>i} |a_{ij}| > |\lambda| (1 + \Delta t \sum_{j>i} |a_{ij}|), \quad (34)$$

which leads to the desired result

$$\rho(\mathbf{C}) < 1 \quad (35)$$

and confirms that, under the stated assumptions, the SDC1 scheme is unconditionally stable.

Remark 4. The condition can be relaxed as \mathbf{A} is diagonally dominant and irreducible with non-positive diagonal entries, when you notice for any $|\lambda| \geq 1$, if \mathbf{A} is diagonally dominant and irreducible, then $\lambda(\mathbf{I} - \Delta t \mathbf{L} - \Delta t \mathbf{D}) - (\mathbf{I} + \Delta t \mathbf{U})$ is diagonally dominant and irreducible [38].

5. Applications

In this section, we present numerical results from a variety of multiphysics systems for the proposed high-order, partitioned spectral deferred correction solver. To demonstrate the high-order accuracy of the solver, we consider a system of ODEs and the time-dependent advection-diffusion-reaction equations. To test the robustness and applicability of the method, we consider two fluid-structure interaction problems, including both incompressible flows and compressible flows.

5.1. Ordinary differential equations system

In this section, we study the proposed high-order partitioned solvers on a stiff 2×2 system of linear ODEs

$$\dot{\mathbf{u}} = \mathbf{A} \mathbf{u}, \quad \mathbf{A} = \begin{bmatrix} 0 & 1 \\ -\alpha & -\alpha - 1 \end{bmatrix}, \quad \mathbf{u} = \begin{bmatrix} u^1 \\ u^2 \end{bmatrix}, \quad (36)$$

with initial condition $\mathbf{u}(0) = (x_0, 0)^T$ and consider the time domain $t \in (0, 20]$. The eigenvalues of \mathbf{A} are -1 and $-\alpha$, therefore, when $\alpha \gg 0$, the system is very stiff. The exact solution at any time t is

$$\begin{bmatrix} u^1(t) \\ u^2(t) \end{bmatrix} = \begin{bmatrix} x_0 \left(-\frac{1}{\alpha-1} \exp^{-\alpha t} + \frac{\alpha}{\alpha-1} e^{-t} \right) \\ x_0 \left(\frac{\alpha}{\alpha-1} \exp^{-\alpha t} - \frac{\alpha}{\alpha-1} e^{-t} \right) \end{bmatrix}. \quad (37)$$

To conform to the multiphysics formulation in eq. (3), the ODE system is treated as a coupled system with three subsystems. The mass matrix is identity, the residual term is taken as

$$\mathbf{r} = (\mathbf{c}^1, (-\alpha - 1)\mathbf{u}^2 + \mathbf{c}^2)^T, \quad (38)$$

and the coupling terms are defined as

$$\mathbf{c}^1 = \mathbf{u}^2, \quad \mathbf{c}^2 = -\alpha \mathbf{u}^1. \quad (39)$$

This decomposition of the residual term is non-unique. In fact, many other choices exist that will lead to different schemes.

The maximum stable time steps Δt_{\max} of monolithic forward Euler approach and the partitioned SDC1 approach¹ with respect to α are $\min\{\frac{2}{\alpha}, 2\}$ and $\frac{\alpha+1+\sqrt{(\alpha+1)^2+4\alpha}}{\alpha}$. It is worth mentioning the maximum stable time step of SDC1 is independent of α and always greater than 1, which indicates our scheme is stable even some fast physical time scales are unresolved.

To test the stability and verify the temporal convergence of the partitioned schemes, we take $\alpha = 1000$ and $x_0 = 1000$. Solutions till $t = 20.0$ obtained by these partitioned SDC schemes introduced in section 4.1 with $\Delta t = 1.0$ are depicted in fig. 1, which indicates all schemes are stable. The order of accuracy is quantified via the L_∞ -norm of the error in the numerical solution at time $t = 20.0$

$$e_{\text{ODE}} = \max_{1 \leq i \leq 2} |\mathbf{u}_N^i - \mathbf{u}^i(20)|, \quad (40)$$

where $\mathbf{u}^i(20)$ is the exact solution at $t = 20.0$ and \mathbf{u}_N^i the numerical solution at the final time step for the i th subsystem. The error e_{ODE} as a function of the time step size for different SDC schemes are shown in fig. 2. The design order of accuracy is achieved. It is worth mentioning that SDC3-r with modified low-order approximation can still lead to third order accuracy as discussed in section 4.2, but the error is slightly larger than that of SDC3-l scheme.

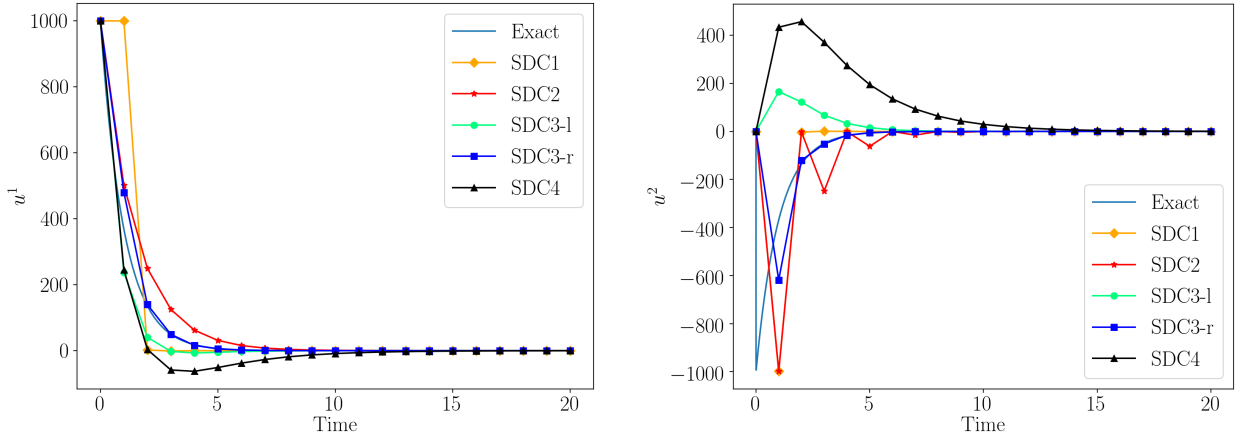


Figure 1: Solutions of the ODE system ($\alpha = 1000$) obtained by partitioned SDC schemes with $\Delta t = 1.0$.

5.2. Advection-diffusion-reaction system

In this section, we consider time-dependent coupled advection-diffusion-reaction (ADR) systems. These systems have applications in the modeling of chemical reactions [39], the description for superconductivity of liquids [40], and biological predator-prey models [41]. In this work, we consider the 2-dimensional predator-prey model from [41], which involves 2 coupled systems. The governing equation for the i th species is

$$\frac{\partial u^i}{\partial t} + (\mathbf{v}^i \cdot \nabla) u^i - \nabla \cdot (D^i \nabla u^i) = f^i(u, x, t), \quad (x, t) \in \Omega \times (0, 1], \quad i = 1, 2. \quad (41)$$

¹A detailed analytical comparison of the monolithic forward Euler scheme, the partitioned SDC1 scheme, and the fixed point iteration scheme on this model ODE problem is presented in Appendix Appendix A.

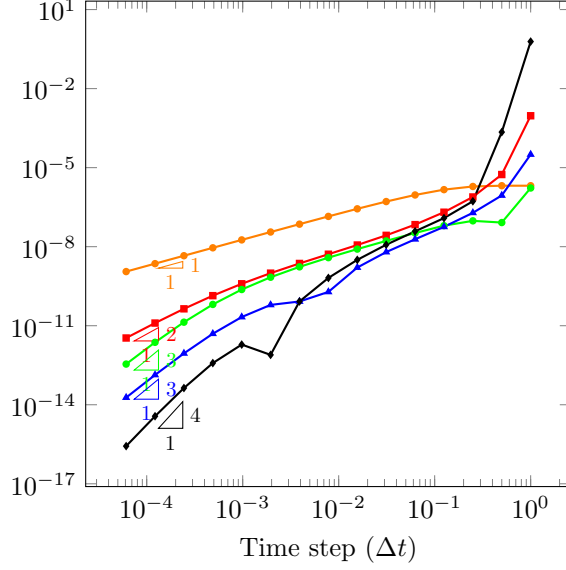


Figure 2: Convergence of the SDC1 (—○—), SDC2 (—■—), SDC3-l (—▲—), SDC3-r (—●—), and SDC4 (—●—) schemes applied to the ODE system.

Here u^1 denotes the prey, u^2 denotes the predator, $u = [u^1, u^2]$, $\Omega \subset \mathbb{R}^2$ is the computational domain. D^i is the diffusivity, and $v^i(x) \in \mathbb{R}^2$ is the velocity field for the i th species. The reaction terms are

$$f^1(u, x, t) = u^1(-(u^1 - a^1)(u^1 - 1) - a^2 u^2) \quad f^2(u, x, t) = u^2(-a^3 - a^4 u^2 + a^2 u^1), \quad (42)$$

where $a^1 = 0.25$, $a^2 = 2$, $a^3 = 1$, $a^4 = 3.4$, and the diffusivities are constant $D^1 = D^2 = 0.01$. The computational domain is the two-dimensional unit square $\Omega = [-0.5, 0.5] \times [-0.5, 0.5]$ with the prey initially uniformly distributed, and predators initially gathered near $(x_0, y_0) = (-0.25, -0.25)$

$$u^1(x, y, 0) = 1.0 \quad \text{and} \quad u^2(x, y, 0) = \begin{cases} 0 & r > d \\ e^{-\frac{d^2}{d^2 - r^2}} & r \leq d \end{cases}, \quad (43)$$

where $d = 0.2$, $r = \sqrt{(x - x_0)^2 + (y - y_0)^2}$. The boundary conditions are all Neumann conditions $\frac{\partial u}{\partial n} = 0$ and the velocity fields are constant $v^1(x) = (0, 0)$ and $v_2(x) = (0.5, 0.5)$. The equations are discretized with a standard high-order discontinuous Galerkin method using upwind flux for the inviscid numerical flux and the compact DG flux [42] for the viscous numerical flux on a 40×40 structured mesh of quadratic simplex elements. The governing equations in (41) reduce to the following system of ODEs after the DG discretization is applied

$$\mathbf{M}^i \dot{\mathbf{u}}^i = \mathbf{r}^i(\mathbf{u}^i) + \mathbf{c}^i(\mathbf{u}^1, \mathbf{u}^2), \quad (44)$$

where \mathbf{M}^i is the fixed mass matrix, $\mathbf{u}^i(t)$ is the semi-discrete state vector, i.e., the discretization of u on Ω , $\mathbf{r}^i(\mathbf{u}^i)$ is the spatial discretization of the advection and diffusion terms on Ω , and \mathbf{c}^i is the coupling term that contains the DG discretization of the i th reaction source term in (42). The solution of (44) using the SDC4 scheme is provided in fig. 3 using the time step size $\Delta t = 0.1$. The predators are diffused quickly and migrate diagonally upward, while the prey are mostly affected by the coupled reaction near the extent of the predator population.

To validate the temporal convergence of the high-order partitioned scheme, we apply these SDC schemes introduced in section 4.1 and, similar to the previous section, we use the L_∞ -error between a reference solution and the numerical solution at time $t = 1.0$ to quantify the error where the reference solution at $t = 1.0$ obtained by using the SDC4 scheme with $\Delta t = 6.25 \times 10^{-3}$. The errors as a function of the time step size are provided in fig. 4, which verifies the design order of accuracy of all SDC schemes. This figure also shows that no stability issues were observed for any of the results, even for the coarsest time step $\Delta t = 0.1$.

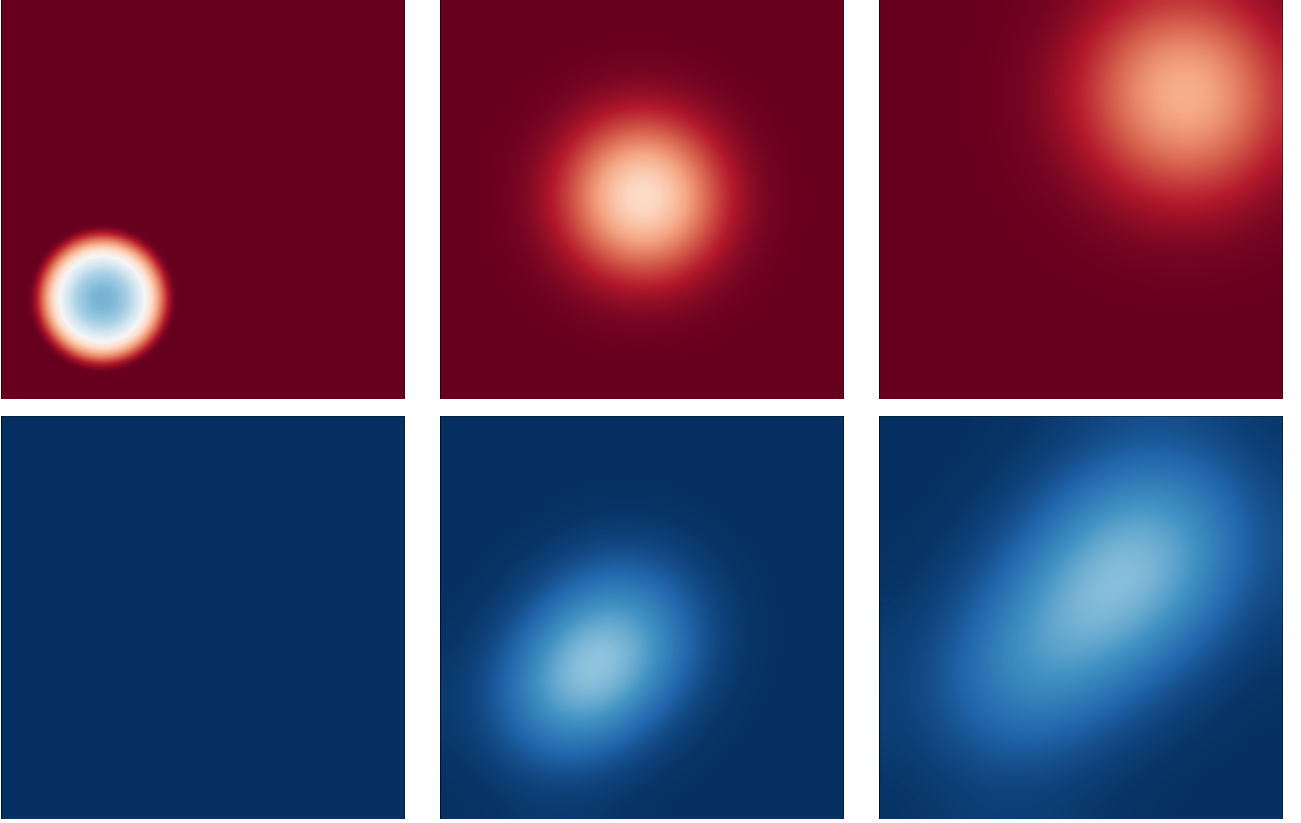


Figure 3: Predator (*top*) and prey (*bottom*) populations at various snapshots in time: $t = 0.0$ (*left*), $t = 0.5$ (*center*), and $t = 1.0$ (*right*).

5.3. Modified cavity problem

In this section, we study the modified driven cavity problem with flexible bottom² depicted in fig. 5. This problem was first introduced in [43] and since then has been used as a benchmark problem for a variety of FSI studies [44, 16, 45, 46, 47]. An oscillating velocity $\mathbf{v}(t) = (1 - \cos(2\pi t/5), 0)$ is imposed on the top of the cavity. Each side is of length 1 containing three elements (two unconstrained nodes) that allow free inflow and outflow of fluid, i.e. homogeneous Neumann boundary conditions are imposed on these apertures. This way the structural displacements are not constrained by the fluid's incompressibility [48]. The fluid density and dynamic viscosity are $\rho^f = 1$ and $\mu^f = 0.01$. The structure is of thickness $h = 0.002$ and Young's modulus $E = 250$. The density of the structure varies for different test cases to demonstrate the stability of the coupling procedures. Decreasing structure density increases difficulties to the coupling algorithm since the main resistance of the structure against the fluid pressure stems from its mass.

The considered Newtonian fluid is governed by the incompressible Navier-Stokes equations [49], written on the undeformed fluid domain Ω_0^f ,

$$\begin{aligned}
 \frac{\partial \mathbf{v}}{\partial t} + (\mathbf{v} - \mathbf{d}^x) : \nabla_x \mathbf{v} - \nabla_x : \frac{\boldsymbol{\sigma}^f}{\rho^f} &= 0 & \text{in } \Omega_0^f, \\
 \nabla_x \cdot \mathbf{v} &= 0 & \text{in } \Omega_0^f, \\
 \mathbf{v}(t) &= \mathbf{v}_D(t) & \text{in } \Gamma_{0D}^f, \\
 \boldsymbol{\sigma}^f \cdot \mathbf{N} &= 0 & \text{in } \Gamma_{0N}^f.
 \end{aligned} \tag{45}$$

Here \mathbf{v} denotes the fluid velocity field, \mathbf{d}^x denotes the mesh velocity, $\boldsymbol{\sigma}^f = -\mu^f(\nabla_x \mathbf{u} + \nabla_x \mathbf{u}^T) + p\mathbb{I}$ denotes the stress

²The detailed implementation of the modified cavity problem is in https://zhengyu_huang@bitbucket.org/zhengyu_huang/incompressible_fsi_2d.git.

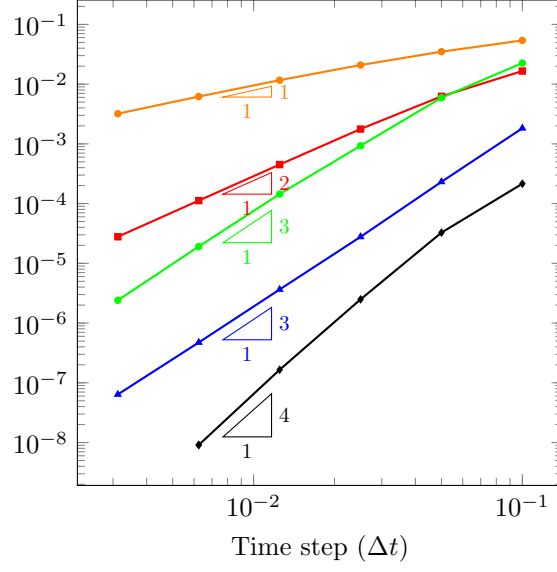


Figure 4: Convergence of the SDC1 (—○—), SDC2 (—■—), SDC3-l (—▲—), SDC3-r (—●—), and SDC4 (—◆—) schemes applied to the predator-prey model.

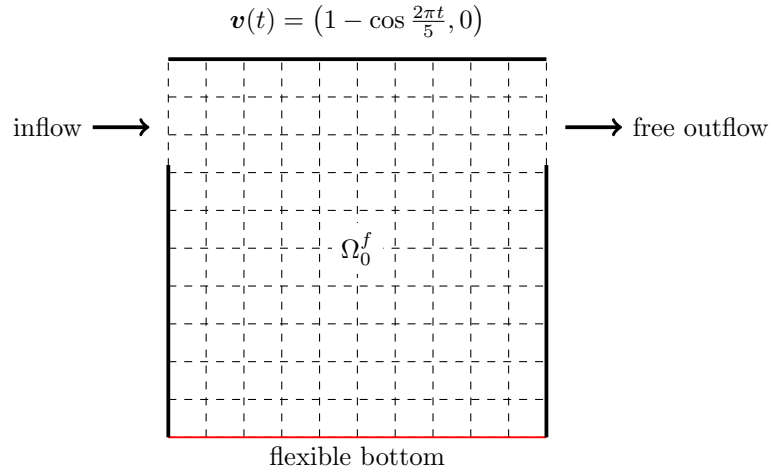


Figure 5: Schematics of the modified cavity problem.

tensor, and p denotes the pressure field. The time derivative in eq. (45) describes the temporal change of velocity on a reference point while all spatial derivatives refer to the deformed domain. Dirichlet boundaries are imposed on both top and bottom, and two side walls denoted as Γ_{0D}^f , and homogeneous Neumann boundary conditions are imposed on both apertures, with outward normal \mathbf{N} and ambient pressure 0.

The governing equations in (45) is semi-discretized by 32×32 traditional Taylor-Hood Q_2 - Q_1 mixed elements, i.e. continuous biquadratic velocity and continuous bilinear pressure, which satisfies the Babuška-Brezzi condition [50, p. 286]. This leads to the following system of ODEs,

$$\mathbf{M}^f \dot{\mathbf{u}}^f = \mathbf{r}^f(\mathbf{u}^f, \mathbf{c}^f), \quad (46)$$

where \mathbf{M}^f is the fixed mass matrix, $\mathbf{u}^f(t)$ is the semi-discrete fluid state vector, i.e. the discretization of \mathbf{v} and p on $\Omega^f(t)$, $\mathbf{r}^f(\mathbf{u}^f, \mathbf{c}^f)$ denotes the spatial discretization of the inviscid and viscous fluxes on Ω_0^f , and \mathbf{c}^f is the coupling term that contains information about the mesh position \mathbf{d}^x and velocities $\dot{\mathbf{d}}^x$. It is worth mentioning that the mass matrix \mathbf{M}^f is singular due to the incompressibility constraints, which causes the added mass effect instability [20, 44, 51] for incompressible flows.

The flexible bottom, with fixed ends, is modeled as the nonlinear beam written in the Lagrangian form in the undeformed domain Ω_0^s . The equilibrium equation of the beam in the weak form can be written as [52, p. 308]

$$\int_{\Omega_0^s} \rho^s \ddot{\mathbf{d}}^s \delta \mathbf{d}^s dX + \int_{\Omega_0^s} \sigma_{11}^s \delta \epsilon_{11}^s dX = \mathbf{f}_{ext} \delta \mathbf{d}^s. \quad (47)$$

Here the first term is the contribution of the inertial forces, the second and third terms represent the virtual work of the internal forces and the external forces. σ_{11}^s and ϵ_{11}^s are nonlinear axial strain and axial stress components, related by the linear elasticity constitutive relation.

The flexible bottom is discretized by 32 beam elements with linear shape functions for the horizontal displacement and cubic Hermitian shape functions for the vertical displacement. The discretized equation becomes

$$\mathbf{M}^s \dot{\mathbf{u}}^s = \mathbf{r}^s(\mathbf{u}^s, \mathbf{c}^s), \quad (48)$$

where \mathbf{M}^s is the fixed mass matrix, $\mathbf{u}^s(t)$ is the semi-discrete state vector consisting of the displacements and velocities of the beam nodes, $\mathbf{r}^s(\mathbf{u}^s, \mathbf{c}^s)$ is the spatial discretization of the virtual work and boundary conditions on the reference domain Ω_0^s , and \mathbf{c}^s is the coupling term that contains information about the flow load on the structure.

To determine the deformation of the fluid mesh, the mesh is considered as a linear pseudo-structure [53, 54] driven solely by Dirichlet boundary conditions provided by the displacement of the structure at the fluid-structure interface. The governing equations are given by the continuum mechanics equations in the Lagrangian form with the linear elastic constitutive relation in the undeformed fluid domain Ω_0^x ,

$$\begin{aligned} \rho^x \ddot{\mathbf{d}}^x - \nabla_X : \boldsymbol{\sigma}^x &= 0 & \text{in } \Omega_0^x, \\ \mathbf{d}^x &= \mathbf{d}_D(t) & \text{on } \partial\Omega_{0D}^x, \\ \dot{\mathbf{d}}^x &= \dot{\mathbf{d}}_D(t) & \text{on } \partial\Omega_{0D}^x, \end{aligned} \quad (49)$$

where $\rho^x = 500$ is the density, and $\boldsymbol{\sigma}^x$ is the Cauchy stress tensor. The position and velocity of the fluid domain are prescribed along $\partial\Omega_{0D}^x$, the union of the fluid-structure interface and the fluid domain boundary.

The governing equations given by (49) are discretized with 32×32 biquadratic elements and reduced to the following system of ODEs,

$$\mathbf{M}^x \dot{\mathbf{u}}^x = \mathbf{r}^x(\mathbf{u}^x, \mathbf{c}^x), \quad (50)$$

where \mathbf{M}^x is the fixed mass matrix, \mathbf{u}^x is the semi-discrete state vector consisting of the displacements and velocities of the mesh nodes, $\mathbf{r}^x(\mathbf{u}^x, \mathbf{c}^x)$ is the spatial discretization of the continuum equations and boundary conditions on the reference domain Ω^x , and \mathbf{c}^x is the coupling term that contains information about the motion of the fluid structure interface.

Finally, we obtain the three-field coupled fluid-structure equations

$$\mathbf{M}^s \dot{\mathbf{u}}^s = \mathbf{r}^s(\mathbf{u}^s, \mathbf{c}^s), \quad \mathbf{M}^x \dot{\mathbf{u}}^x = \mathbf{r}^x(\mathbf{u}^x, \mathbf{c}^x), \quad \mathbf{M}^f \dot{\mathbf{u}}^f = \mathbf{r}^f(\mathbf{u}^f, \mathbf{c}^f). \quad (51)$$

The coupling terms have the following dependencies

$$\mathbf{c}^s = \mathbf{c}^s(\mathbf{u}^s, \mathbf{u}^x, \mathbf{u}^f), \quad \mathbf{c}^x = \mathbf{c}^x(\mathbf{u}^s), \quad \mathbf{c}^f = \mathbf{c}^f(\mathbf{u}^s, \mathbf{u}^x). \quad (52)$$

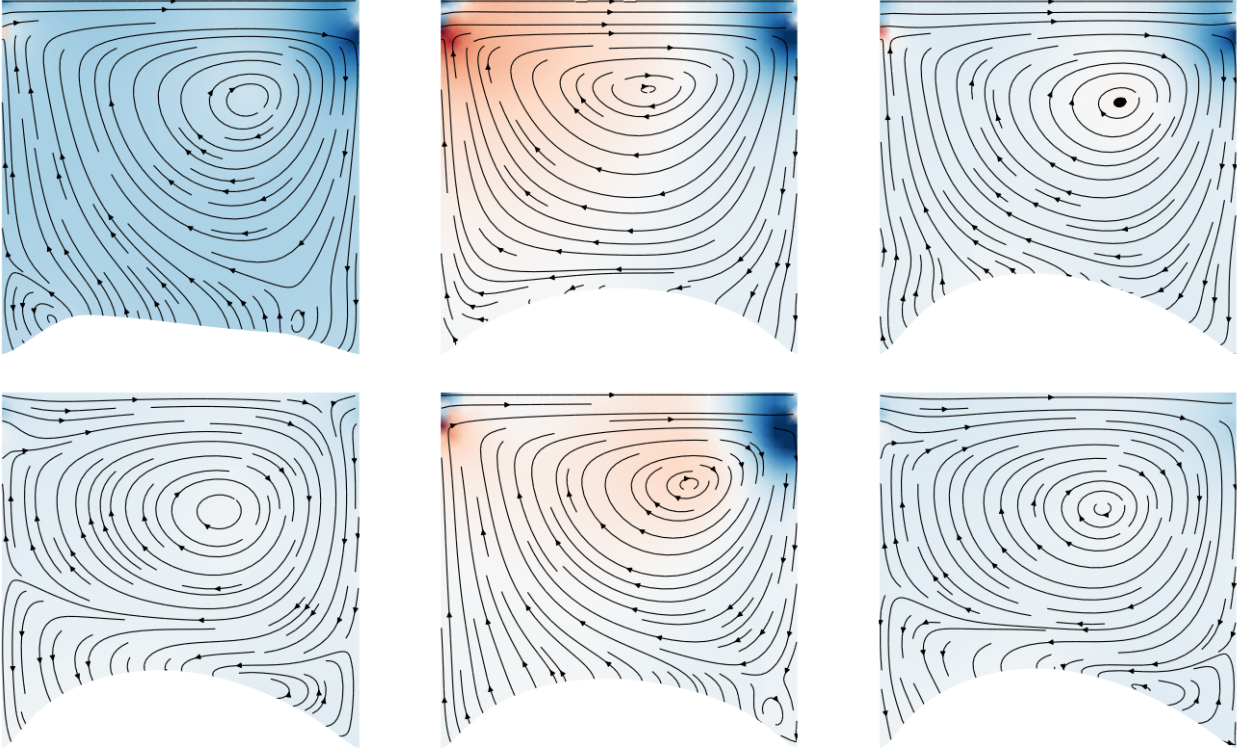


Figure 6: Driven cavity pressure field and velocity streamlines $t=4, 22, 44, 65, 83, 100$ (left-to-right, top-to-bottom).

The ordering of the subsystems implied in eq. (51) is used throughout the remainder of this section, which plays an important role when defining the Gauss-Seidel predictors—only a single predictor $\tilde{\mathbf{c}}^s$ is needed to decouple the multiphysics system. The conservative load and motion transfer algorithms [55] are applied to evaluate these coupling terms.

The aforementioned SDC solvers are applied to this benchmark problem, The time step is fixed to be 0.1, the simulation time is $T = 100$ (20 periods), and the Young’s modulus and Poisson’s ratio of the pseudo-structure are set to be 250 and 0.0. The flow is initially quiescent with 0 pressure, the same as the ambient pressure. Snapshots of the pressure field and the streamlines are shown in fig. 6, with the structure density $\rho^s = 500$. The flexible bottom undergoes large deformations and oscillates along with the prescribed periodic velocity at the top. To understand the stability of the proposed partitioned solvers, we vary the density of the structure ρ^s by multiples of one hundred. The minimal structure density that leads to a stable simulation for different SDC schemes are reported in table 1. The corresponding vertical displacements of the central point on the flexible bottom are depicted in fig. 7, no spurious oscillations are observed, which indicates numerical stability. Here the backward Euler scheme (BE) is from [44], which solves the incompressible flow by using the backward Euler scheme, and the structure with generalized- α time integration scheme [56, 44]. Its sequentially staggered algorithm (no iterations) is equipped with a first order structure displacement predictor, which is the most stable partitioned solver reported in [44]. Its minimal stable structure density in the present setup is 900, which outperforms the SDC1 scheme, thanks to the improved numerical dissipation from the generalized- α time integration scheme. However, SDC2 and SDC3-r schemes are stable with $\rho^s = 500$ and $\rho^s = 400$, which demonstrates the superior stability of the proposed high order partitioning solvers. And SDC3-r scheme is the most stable scheme for this test case, which demonstrates the possibility to improve stability through judiciously choosing the low order approximation \mathcal{C}_j . Moreover, it is worth mentioning that IMEX based high order partitioned solvers [1] can not handle this case, due to the singular fluid mass matrix; more comparisons will be presented in section 5.4.

Method	BE	SDC1	SDC2	SDC3-l	SDC3-r	SDC4
ρ^s	900	1200	500	800	400	1000

Table 1: Minimum structure density to maintain the stability of the modified cavity flow problem for different schemes.

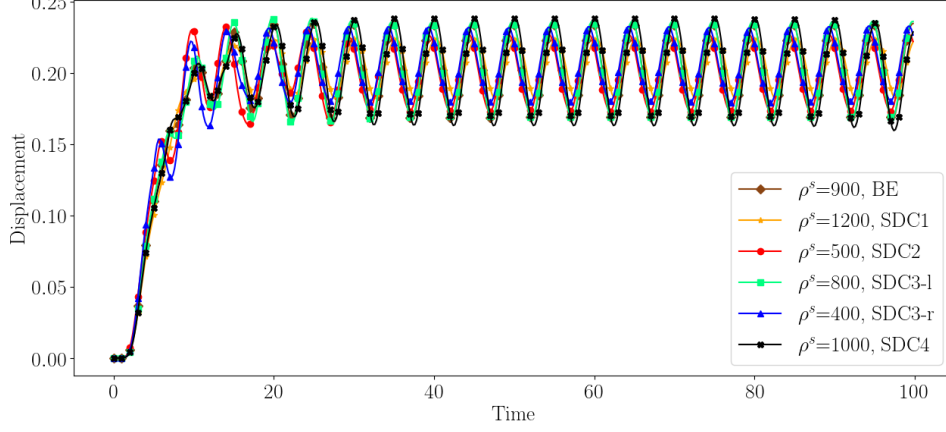


Figure 7: Displacement of the central point at the flexible bottom of the cavity for different schemes at the minimum stable density.

5.4. Foil damper problem

In this section, we demonstrate the proposed SDC solvers on the energy-harvesting model problem [57, 58, 1]. Consider the foil-damper system in fig. 8 suspended in an isentropic, viscous flow where the rotational motion is a prescribed periodic motion $\theta(t) = \frac{\pi}{4} \cos(2\pi ft)$ with frequency $f = 0.2$ and the vertical displacement is determined by balancing the forces exerted on the airfoil by fluid and damper.

The considered Newtonian fluid is governed by the compressible Navier-Stokes equations, defined on a deformable fluid domain $\Omega^f(t)$, which can be written as a viscous conservation law

$$\frac{\partial U}{\partial t} + \nabla_x \cdot \mathcal{F}^{inv}(U) + \nabla_x \cdot \mathcal{F}^{vis}(U, \nabla_x U) = 0 \quad \text{in } \Omega^f(t), \quad (53)$$

where U is the conservative state variable vector and the physical flux consists of an inviscid part $\mathcal{F}^{inv}(U)$ and a viscous part $\mathcal{F}^{vis}(U, \nabla_x U)$,

$$U = \begin{bmatrix} \rho^f \\ \rho^f \mathbf{v} \\ E \end{bmatrix}, \quad \mathcal{F}^{inv}(U) = \begin{bmatrix} \rho^f \mathbf{v} \\ \rho^f \mathbf{v} \otimes \mathbf{v} + p\mathbb{I} \\ (E + p)\mathbf{v} \end{bmatrix}, \quad \text{and } \mathcal{F}^{vis}(U, \nabla U) = \begin{bmatrix} 0 \\ \boldsymbol{\tau} \\ \boldsymbol{\tau} \cdot \mathbf{v} - \mathbf{q} \end{bmatrix}, \quad (54)$$

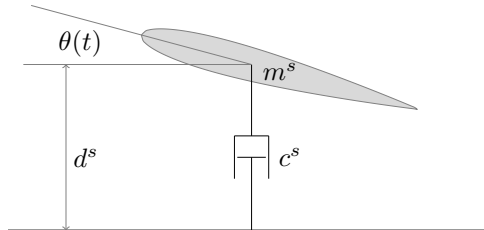


Figure 8: Schematics of the foil-damper system.

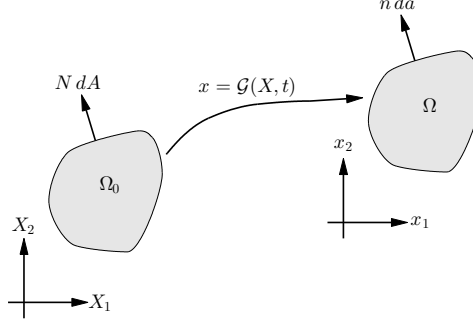


Figure 9: Mapping between reference and physical domains.

here ρ^f is the fluid density, \mathbf{v} is the velocity, and E is the total energy per unit volume. The stress tensor and the heat flux are given by

$$\boldsymbol{\tau} = -\frac{2}{3}\mu^f(\nabla \cdot \mathbf{v})\mathbb{I} + \mu^f(\nabla \mathbf{v} + \nabla \mathbf{v}^T), \quad \mathbf{q} = -\kappa \nabla T, \quad (55)$$

where μ^f is the dynamic viscosity, and κ is the thermal conductivity, and T is the temperature. The isentropic assumption states the entropy of the system is assumed constant, which is tantamount to the flow being adiabatic and reversible. For a perfect gas, the entropy is defined as

$$s = p/(\rho^f)^\gamma, \quad (56)$$

here γ is the specific heat ratio.

The conservation law in (53) is transformed to a fixed reference domain Ω_0^f by defining a time-dependent diffeomorphism \mathcal{G} between the reference domain and physical domain; see fig. 9. At each time t , a point X in the reference domain Ω_0^f is mapped to $x(X, t) = \mathcal{G}(X, t)$ in the physical domain $\Omega^f(t)$. The deformation gradient G , velocity v_G , and Jacobian g of the mapping are defined as

$$G = \nabla_X \mathcal{G}, \quad v_G = \frac{\partial \mathcal{G}}{\partial t}, \quad g = \det G. \quad (57)$$

Following the procedure in [59, 58], the governing equation (53) can be written in the reference domain as

$$\frac{\partial U_X}{\partial t} + \nabla_X \cdot \mathcal{F}_X^{inv}(U_X) + \nabla_X \cdot \mathcal{F}_X^{vis}(U_X, \nabla_X U_X) = 0 \quad \text{in } \Omega_0^f, \quad (58)$$

where ∇_X defines the spatial derivative with respect to the reference domain, conserved quantities and its derivatives in the reference domain are written as

$$U_X = gU, \quad \nabla_X U_X = g\nabla_x U \cdot G + g^{-1}U_X \frac{\partial g}{\partial X}. \quad (59)$$

The inviscid and viscous fluxes are transformed to the reference domain as

$$\begin{aligned} \mathcal{F}_X^{inv}(U_X) &= g\mathcal{F}^{inv}(g^{-1}U_X)G^{-T} - gU_X \otimes v_G G^{-T}, \\ \mathcal{F}_X^{vis}(U_X) &= g\mathcal{F}^{vis}\left(g^{-1}U_X, g^{-1}\left[\nabla_X U_X - g^{-1}U_X \frac{\partial g}{\partial X}\right]G^{-1}\right)G^{-T}. \end{aligned} \quad (60)$$

The governing equations given by (58) are discretized with a standard high-order discontinuous Galerkin method using Roe's flux [60] for the inviscid numerical flux and the compact DG flux [42] for the viscous numerical flux. The DG discretization uses a mesh consisting of 3912 cubic simplex elements, and leads to the following system of ODEs

$$\mathbf{M}^f \dot{\mathbf{u}}^f = \mathbf{r}^f(\mathbf{u}^f, \mathbf{c}^f), \quad (61)$$

where \mathbf{M}^f is the fixed mass matrix, $\mathbf{u}^f(t)$ is the semi-discrete fluid state vector, i.e., the discretization of U_X on Ω_0^f , $\mathbf{r}^f(\mathbf{u}^f, \mathbf{c}^f)$ is the spatial discretization of the transformed inviscid and viscous fluxes on Ω_0^f , and \mathbf{c}^f is the coupling

term that contains information about the domain mapping $\mathcal{G}(X, t)$. In particular, the coupling term contains the position and velocities of the nodal coordinates of the computational mesh. The domain mapping is defined using a nodal (Lagrangian) basis.

The foil is modeled as a simple mass-spring-damper system that can directly be written as a second-order system of ODEs, with respect to the vertical displacement d^s , as follows,

$$m^s \ddot{d}^s + c^s \dot{d}^s + k^s d^s = f_{ext}(t), \quad (62)$$

where m^s is the mass of the (rigid) object, $c^s = 1$ is the damper resistance constant, $k^s = 0$ is the spring stiffness, and $f_{ext}(t)$ is a time-dependent external load, which will be given by integrating the pointwise force the fluid exerts on the object. This simple structure allows us to study the stability and accuracy properties of the proposed high-order partitioned solver for this class of multiphysics problems without the distraction of transferring solution fields across the fluid-structure interface.

To conform to the notation in this document and encapsulate the semi-discretization of PDE-based structure models, the equation in (62) is re-written in a first-order form as

$$\mathbf{M}^s \dot{\mathbf{u}}^s = \mathbf{r}^s(\mathbf{u}^s, \mathbf{c}^s). \quad (63)$$

In the case of the simple structure in (62), the mass matrix, state vector, residual, and coupling term are

$$\mathbf{M}^s = \begin{bmatrix} m^s & \\ & 1 \end{bmatrix}, \quad \mathbf{u}^s = \begin{bmatrix} d^s \\ \dot{d}^s \end{bmatrix}, \quad \mathbf{c}^s = f_{ext}, \quad \mathbf{r}^s(\mathbf{u}^s, \mathbf{c}^s) = \begin{bmatrix} f_{ext} - c^s \dot{d}^s - k^s d^s \\ \dot{d}^s \end{bmatrix}. \quad (64)$$

The motion of the fluid mesh is described as a blending map [59]. That is, the domain mapping $x = \mathcal{G}(X, t)$ is given by an analytical function, parametrized by the deformation and velocity of the fluid-structure interface, that can be analytically differentiated to obtain the deformation gradient $G(X, t)$ and velocity $v_G(X, t)$. Since the fluid mesh motion is no longer included in the system of time-dependent partial differential equations, this leads to a two-field FSI formulation in terms of the fluid and structure states only.

In the two-field FSI setting

$$\mathbf{M}^s \dot{\mathbf{u}}^s = \mathbf{r}^s(\mathbf{u}^s, \mathbf{c}^s), \quad \mathbf{M}^f \dot{\mathbf{u}}^f = \mathbf{r}^f(\mathbf{u}^f, \mathbf{c}^f), \quad (65)$$

the mesh motion is given by an analytical function and the coupling terms have the following dependencies

$$\mathbf{c}^s = \mathbf{c}^s(\mathbf{u}^s, \mathbf{u}^f), \quad \mathbf{c}^f = \mathbf{c}^f(\mathbf{u}^s). \quad (66)$$

In this case, the structure coupling term is determined from the fluid and structure state since the external force depends on the traction integrated over the fluid-structure interface. The fluid coupling term, i.e., the position and velocity of the fluid mesh, is determined from the structure state. Finally, the ordering is chosen as in section 5.3, and only a single predictor $\tilde{\mathbf{c}}^s$ is needed to decouple the multiphysics system.

Snapshots of the vorticity field and motion of the airfoil are shown in fig. 10 for a single configuration of the fluid-structure system. Our numerical experiments study the stability of the proposed SDC partitioned schemes as a function of the mass ratio between the structure and fluid, an important parameter that can impact the stability of partitioned solvers as identified in [20, 23], and the time step size for SDC schemes up to fourth order. The mass ratio, \bar{m} , considered is the ratio of the mass of the structure, m^s , to the mass of fluid displaced by the structure, $\rho^f A$, where $A = 0.08221$ is the area of the airfoil. Since the isentropic Navier-Stokes equations can be seen as an artificial compressibility formulation for the incompressible Navier-Stokes equations [61, 62], we consider the reference fluid density to be constant and equal to the freestream density $\rho^f = 1$. Variations in the mass ratio are achieved by varying the mass of the structure with all other parameters fixed. The stability results are summarized in fig. 11 where \blacktriangle indicates a $(\Delta t, \bar{m})$ -pair that leads to a stable simulation and \blacksquare leads to an unstable one. The corresponding foil vertical displacements for these blue dots adjacent to these unstable red dots are depicted in fig. 12; no trail of unstable oscillation appears.

Figure 11 also shows that all schemes are stable once the time step is sufficiently small, at least for this range of mass ratios considered. The SDC3-r scheme is the most robust scheme, which is the same as the result in section 5.3. Moreover, by comparing with the IMEX based partition solvers in [1], which is reproduced in fig. 13, we conclude the SDC-based partition schemes are more robust for all temporal orders. Finally, the efficiency of these two arbitrarily high-order partitioned solvers is also studied, in terms of the number of implicit solvings, which are listed in table 2. The IMEX schemes are more efficient than SDC schemes in terms of implicit solves; however, potential improvement for SDC would be parallel-in-time evaluation, using an algorithm such as PFASST [63].

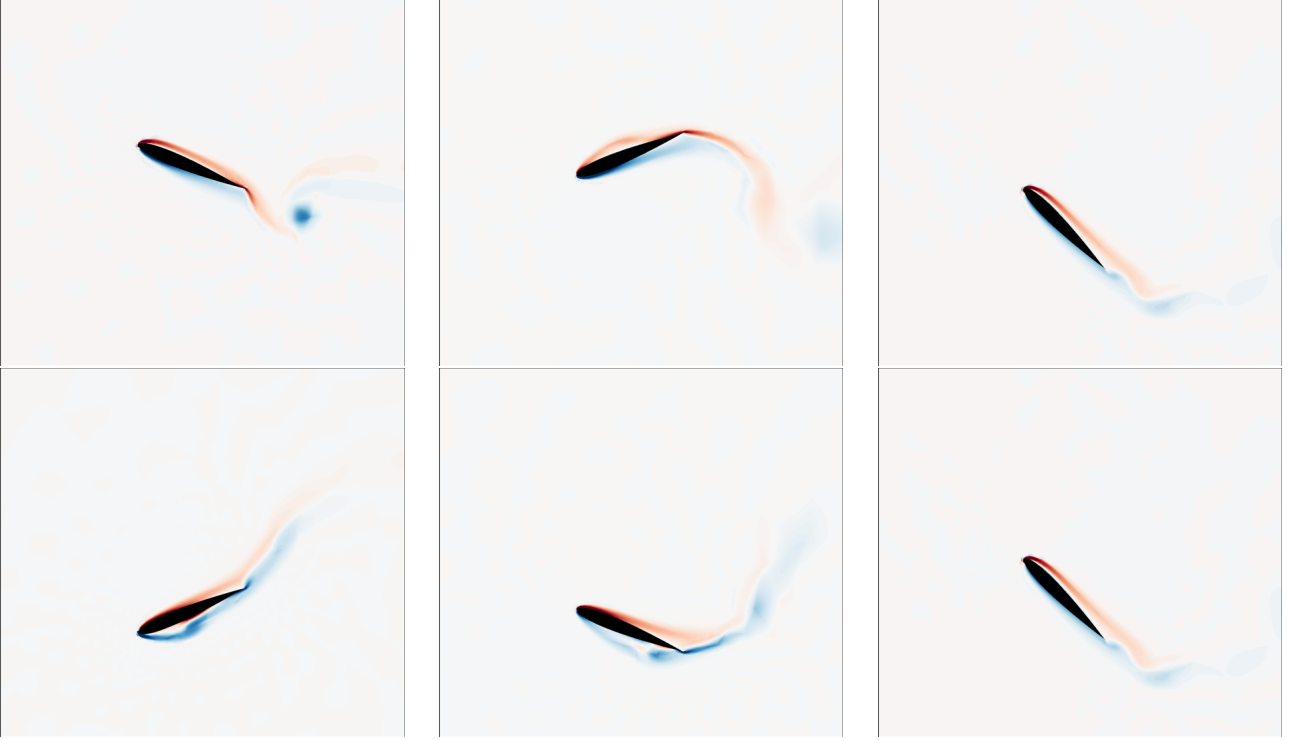


Figure 10: Airfoil motion and flow vorticity corresponding to foil-damper system under prescribed rotational motion $\theta(t) = \frac{\pi}{4} \cos(2\pi ft)$ with frequency $f = 0.2$ at various snapshots in time: $t = 0.83, 1.67, 2.5, 3.33, 4.17, 5.0$ (left-to-right, top-to-bottom) with $m^s = 1$, $\Delta t = 0.025$, and SDC4 scheme.

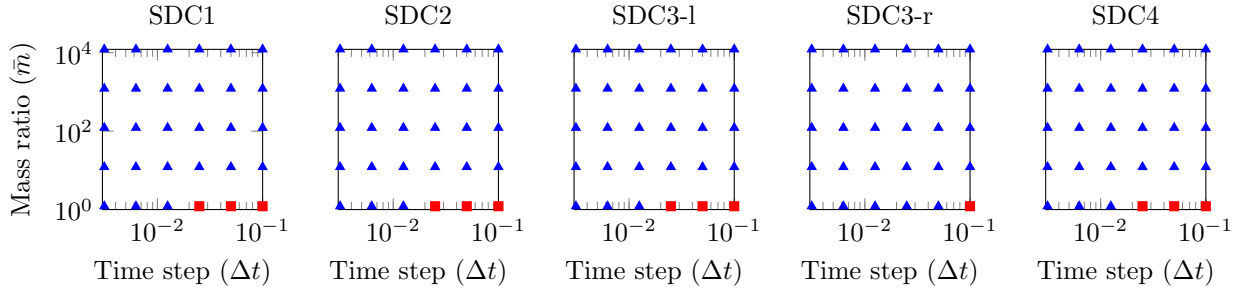


Figure 11: Behavior of the predictor-based partitioned schemes for a range of mass ratios and time steps for SDC1, SDC2, SDC3-l, SDC3-r, and SDC4 (left to right) schemes. Legend: \blacktriangle indicates a stable simulation and \blacksquare indicates an unstable simulation.

Method	BE	SDC1	SDC2	SDC3-l/r	SDC4	IMEX1	IMEX2	IMEX3	IMEX4
Implicit fluid solve	1	1	2	6	8	1	1	3	5
Implicit structure solve	1	1	2	6	8	1	1	3	5

Table 2: Number of Implicit solvings during one time step for SDC and IMEX based partitioned solvers

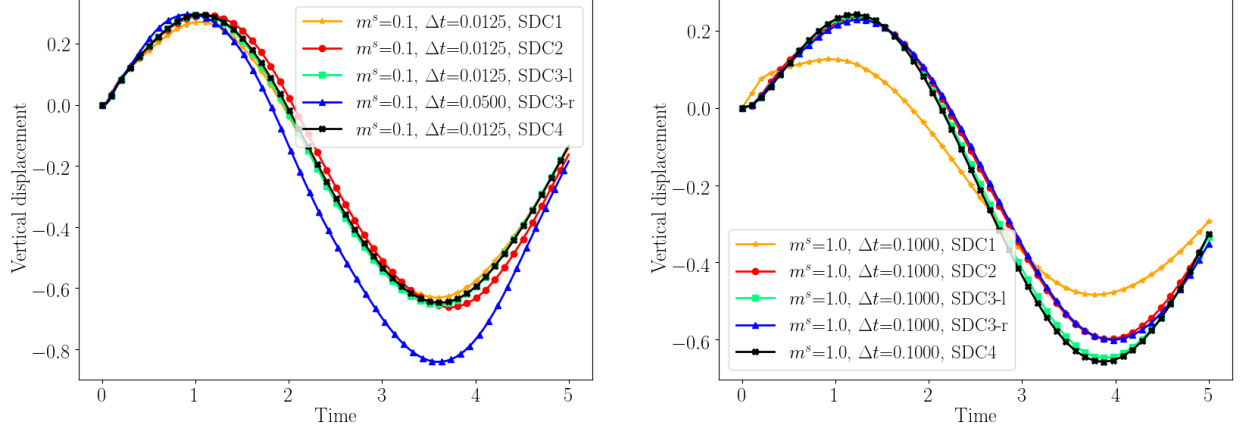


Figure 12: Vertical displacements of the foil for different SDC schemes at the minimum stable structure mass.

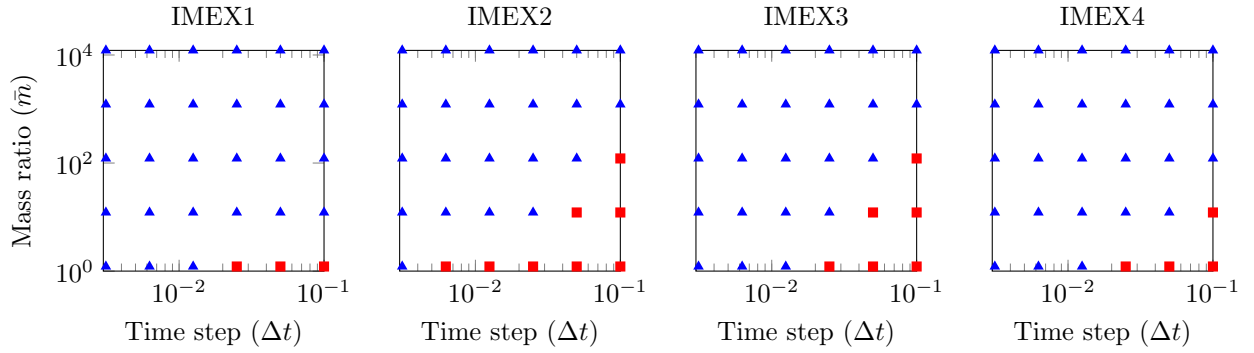


Figure 13: Behavior of the predictor-based partitioned schemes for a range of mass ratios and time steps for IMEX1-IMEX4 (left to right) schemes with the weak Gauss-Seidel predictor. Legend: \blacktriangle indicates a stable simulation and \blacksquare indicates an unstable simulation [1].

6. Conclusion

This paper introduces a framework for constructing high-order, stable, partitioned solvers for general multiphysics problems, whose governing PDEs are first discretized in space only to a set of first-order ODEs. The ODE system is solved by spectral deferred correction methods, wherein arbitrarily high-order accuracy is attained by performing a series of correction sweeps using a low-order solver. When the low-order solver is designed to be partitioned, the corresponding SDC solver is partitioned. Moreover, thanks to these correction sweeps or iterations, the resultant SDC solvers are more stable, which has been demonstrated in the present work. Sufficient conditions to construct consistent low-order solvers are derived and based on these conditions, partitioned multiphysics solvers up to fourth order are constructed, and their properties are analyzed in detail. The stability property of SDC1 is studied based on couple linear model problem, which can be used to guide the design of more robust partitioned solvers. Further stability analysis for different choices of low-order approximation will be considered in the future. The number of implicit solvings increases quadratically along with the increasing of the order of accuracy, how to improve the efficiency is also worth future investigations.

Acknowledgement

Daniel Z. Huang gratefully acknowledges support from the Jet Propulsion Laboratory (JPL) under Contract JPL-RSA No. 1590208. This work was also supported by the National Aeronautics and Space Administration (NASA) under grant number NNX16AP15A. Lawrence Livermore National Laboratory is operated by Lawrence Livermore National Security, LLC, for the U.S. Department of Energy, National Nuclear Security Administration under Contract DE-AC52-07NA27344. LLNL-JRNL-788544.

Appendix A. Analytical comparison of different schemes for the ODE system in Section 5.1

Let $a_{ij}, i = 1, 2, j = 1, 2$ be the entries of the coefficient matrix in the ODE system in Section 5.1, the monolithic forward Euler scheme, the partitioned SDC1 scheme, and the fixed point iteration scheme are analytically studied in this section.

The monolithic forward Euler scheme updates the state as

$$\mathbf{u}_{n+1} = \mathbf{u}_n + \Delta t \mathbf{A} \mathbf{u}_n. \quad (\text{A.1})$$

The update matrix becomes

$$\mathbf{C} = \mathbf{I} + \Delta t \mathbf{A}, \quad (\text{A.2})$$

and its spectrum radius is $\rho(\mathbf{C}) = \max\{|1 - \Delta t|, |1 - \Delta t \alpha|\}$. Therefore, the maximum time step is $\Delta t_{\max} = \min\{\frac{2}{\alpha}, 2\}$.

The partitioned SDC1 scheme (1 iteration) in algorithm 1 updates the state as

$$\begin{aligned} u_{n+1}^1 &= u_n^1 + \Delta t \left((a^{11}u_{n+1}^1 + a^{12}u_n^2) - (a^{11}u_n^1 + a^{12}u_n^2) \right) + \Delta t (a^{11}u_n^1 + a^{12}u_n^2) \\ u_{n+1}^2 &= u_n^2 + \Delta t \left((a^{21}u_{n+1}^1 + a^{22}u_{n+1}^2) - (a^{21}u_n^1 + a^{22}u_n^2) \right) + \Delta t (a^{21}u_n^1 + a^{22}u_n^2). \end{aligned} \quad (\text{A.3})$$

Bringing the parameters in Section 5.1, the update matrix becomes

$$\mathbf{C} = \begin{bmatrix} 1 & \Delta t \\ -\frac{\alpha \Delta t}{1 + \Delta t(\alpha + 1)} & \frac{1 - \alpha \Delta t^2}{1 + \Delta t(\alpha + 1)} \end{bmatrix}, \quad (\text{A.4})$$

and its eigenvalues satisfy

$$\lambda^2 - \left(1 + \frac{1 - \alpha \Delta t^2}{1 + \Delta t(\alpha + 1)}\right) \lambda + \frac{1}{1 + \Delta t(\alpha + 1)} = 0, \quad (\text{A.5})$$

If eq. (A.5) has a pair of complex-conjugate eigenvalues, we have $\lambda_1 \lambda_2 = \frac{1}{1 + \Delta t(\alpha + 1)} < 1$, therefore it is unconditional stable. If eq. (A.5) has positive eigenvalues, eq. (A.5) can be rearranged as

$$(\lambda - 1) \left(\lambda - \frac{1}{1 + \Delta t(\alpha + 1)} \right) + \frac{\alpha \Delta t^2}{1 + \Delta t(\alpha + 1)} \lambda = 0, \quad (\text{A.6})$$

therefore, the positive eigenvalue is smaller than 1. And the only unstable case corresponds to eigenvalues smaller than -1 . Therefore, the maximum time step is $\Delta t_{\max} = \frac{\alpha+1+\sqrt{(\alpha+1)^2+4\alpha}}{\alpha}$.

The fixed point iteration scheme with the same type of Gauss-Seidel coupling starts with a suitably predicted $\tilde{u}_{n+1}^2 = u_n^2$, and solves each subsystem equation

$$\begin{aligned} u_{n+1}^1 &= u_n^1 + \Delta t \left(a^{11} u_{n+1}^1 + a^{12} \tilde{u}_{n+1}^2 \right), \\ u_{n+1}^2 &= u_n^2 + \Delta t \left(a^{21} u_{n+1}^1 + a^{22} u_{n+1}^2 \right). \end{aligned} \tag{A.7}$$

Then it updates the predicted state $\tilde{u}_{n+1}^2 := u_{n+1}^2$ until it converges. The update equation of the fixed point iteration becomes

$$u_{n+1}^2 = \frac{\Delta t^2 a^{12} a^{21}}{(1 - \Delta t a^{11})(1 - \Delta t a^{22})} \tilde{u}_{n+1}^2 + \frac{1}{1 - \Delta t a^{22}} u_n^2 + \frac{\Delta t a^{21}}{(1 - \Delta t a^{11})(1 - \Delta t a^{22})} u_n^1. \tag{A.8}$$

Bringing the parameters in Section 5.1, the fixed point iteration converges with $\Delta t_{\max} = \frac{\alpha+1+\sqrt{(\alpha+1)^2+4\alpha}}{2\alpha}$, and the linear convergence rate is

$$\mathcal{O}\left(\frac{\Delta t^2 \alpha}{1 + \Delta t(\alpha + 1)}\right). \tag{A.9}$$

For this specific ODE model problem, our partitioned SDC1 scheme has larger stable time step. As for high order partitioned SDC schemes, even the iteration number increases quadratically, for 1-st to 4-th order SDC schemes, the iteration numbers might be fewer than that of the fixed point iteration.

References

- [1] D.Z. Huang, P.-O. Persson, and M.J. Zahr. High-order, linearly stable, partitioned solvers for general multiphysics problems based on implicit-explicit Runge-Kutta schemes. *Computer Methods in Applied Mechanics and Engineering*, 346:674–706, April 2019.
- [2] Daniel Z. Huang, Matthew J. Zahr, and Per-Olof Persson. A high-order partitioned solver for general multiphysics problems and its applications in optimization. In *AIAA Scitech 2019 Forum*. American Institute of Aeronautics and Astronautics, January 2019.
- [3] Ramji Kamakoti and Wei Shyy. Fluid–structure interaction for aeroelastic applications. *Progress in Aerospace Sciences*, 40(8):535–558, 2004.
- [4] Xiangying Chen, Ge-Cheng Zha, and Ming-Ta Yang. Numerical simulation of 3-d wing flutter with fully coupled fluid–structural interaction. *Computers & fluids*, 36(5):856–867, 2007.
- [5] Zhengyu Huang, Philip Avery, Charbel Farhat, Jason Rabinovitch, Armen Derkevorkian, and Lee D Peterson. Simulation of parachute inflation dynamics using an eulerian computational framework for fluid-structure interfaces evolving in high-speed turbulent flows. In *2018 AIAA Aerospace Sciences Meeting*, page 1540, 2018.
- [6] Yuri Bazilevs, Victor M Calo, Yongjie Zhang, and Thomas JR Hughes. Isogeometric fluid–structure interaction analysis with applications to arterial blood flow. *Computational Mechanics*, 38(4-5):310–322, 2006.
- [7] Jaroslav Hron and Martin Mádlík. Fluid-structure interaction with applications in biomechanics. *Nonlinear analysis: real world applications*, 8(5):1431–1458, 2007.
- [8] Vincent Chabannes, Gonçalo Pena, and Christophe Prud’homme. High-order fluid–structure interaction in 2d and 3d application to blood flow in arteries. *Journal of Computational and Applied Mathematics*, 246:1–9, 2013.
- [9] Parviz Moin and Sourabh V Apte. Large-eddy simulation of realistic gas turbine combustors. *AIAA journal*, 44(4):698–708, 2006.
- [10] Yen-Sen Chen, TH Chou, BR Gu, JS Wu, Bill Wu, YY Lian, and Luke Yang. Multiphysics simulations of rocket engine combustion. *Computers & Fluids*, 45(1):29–36, 2011.
- [11] Gábor Tóth. The $\nabla \cdot b = 0$ constraint in shock-capturing magnetohydrodynamics codes. *Journal of Computational Physics*, 161(2):605–652, 2000.
- [12] Luis Chacón, Dana A Knoll, and JM Finn. An implicit, nonlinear reduced resistive mhd solver. *Journal of Computational Physics*, 178(1):15–36, 2002.
- [13] Eric C Cyr, John N Shadid, Raymond S Tuminaro, Roger P Pawlowski, and Luis Chacón. A new approximate block factorization preconditioner for two-dimensional incompressible (reduced) resistive mhd. *SIAM Journal on Scientific Computing*, 35(3):B701–B730, 2013.
- [14] Björn Hübner, Elmar Walhorn, and Dieter Dinkler. A monolithic approach to fluid–structure interaction using space–time finite elements. *Computer methods in applied mechanics and engineering*, 193(23):2087–2104, 2004.
- [15] C Michler, SJ Hulshoff, EH Van Brummelen, and René De Borst. A monolithic approach to fluid–structure interaction. *Computers & Fluids*, 33(5):839–848, 2004.
- [16] Ulrich Küttler and Wolfgang A Wall. Fixed-point fluid–structure interaction solvers with dynamic relaxation. *Computational mechanics*, 43(1):61–72, 2008.
- [17] C. Farhat and M. Lesoinne. Two efficient staggered algorithms for the serial and parallel solution of three-dimensional nonlinear transient aeroelastic problems. *Computer Methods in Applied Mechanics and Engineering*, 182(3):499–515, 2000.
- [18] S. Piperno and C. Farhat. Partitioned procedures for the transient solution of coupled aeroelastic problems–Part II: energy transfer analysis and three-dimensional applications. *Computer Methods in Applied Mechanics and Engineering*, 190(24):3147–3170, 2001.

- [19] Santiago Badia, Fabio Nobile, and Christian Vergara. Fluid–structure partitioned procedures based on Robin transmission conditions. *Journal of Computational Physics*, 227(14):7027–7051, 2008.
- [20] Paola Causin, Jean-Frédéric Gerbeau, and Fabio Nobile. Added-mass effect in the design of partitioned algorithms for fluid–structure problems. *Computer Methods in Applied Mechanics and Engineering*, 194(42-44):4506–4527, 2005.
- [21] Xiaolin Zhong. Additive semi-implicit Runge–Kutta methods for computing high-speed nonequilibrium reactive flows. *Journal of Computational Physics*, 128(1):19–31, 1996.
- [22] Uri M Ascher, Steven J Ruuth, and Raymond J Spiteri. Implicit-explicit Runge-Kutta methods for time-dependent partial differential equations. *Applied Numerical Mathematics*, 25(2-3):151–167, 1997.
- [23] AH Van Zuijlen, Aukje de Boer, and Hester Bijl. Higher-order time integration through smooth mesh deformation for 3D fluid–structure interaction simulations. *Journal of Computational Physics*, 224(1):414–430, 2007.
- [24] Bradley Froehle and Per-Olof Persson. A high-order discontinuous Galerkin method for fluid–structure interaction with efficient implicit–explicit time stepping. *Journal of Computational Physics*, 272:455–470, 2014.
- [25] Alok Dutt, Leslie Greengard, and Vladimir Rokhlin. Spectral deferred correction methods for ordinary differential equations. *BIT Numerical Mathematics*, 40(2):241–266, 2000.
- [26] Michael L. Minion. Semi-implicit spectral deferred correction methods for ordinary differential equations. *Communications in Mathematical Sciences*, 1(3):471–500, 2003.
- [27] Anne Bourlioux, Anita T Layton, and Michael L Minion. High-order multi-implicit spectral deferred correction methods for problems of reactive flow. *Journal of Computational Physics*, 189(2):651–675, 2003.
- [28] Thomas Hagstrom and Ruhai Zhou. On the spectral deferred correction of splitting methods for initial value problems. *Communications in Applied Mathematics and Computational Science*, 1(1):169–205, December 2006.
- [29] Mathew Causley and David Seal. On the convergence of spectral deferred correction methods. *Communications in Applied Mathematics and Computational Science*, 14(1):33–64, 2019.
- [30] Andrew Christlieb, Wei Guo, Maureen Morton, and Jing-Mei Qiu. A high order time splitting method based on integral deferred correction for semi-lagrangian vlasov simulations. *Journal of Computational Physics*, 267:7–27, 2014.
- [31] Michael M Crockatt, Andrew J Christlieb, C Kristopher Garrett, and Cory D Hauck. An arbitrary-order, fully implicit, hybrid kinetic solver for linear radiative transport using integral deferred correction. *Journal of Computational Physics*, 346:212–241, 2017.
- [32] Michael L Minion and RI Saye. Higher-order temporal integration for the incompressible navier–stokes equations in bounded domains. *Journal of Computational Physics*, 375:797–822, 2018.
- [33] Will Pazner, Andrew Nonaka, John Bell, Marcus Day, and Michael Minion. A high-order spectral deferred correction strategy for low Mach number flow with complex chemistry. *Combustion Theory and Modeling*, 20(3):521–547, 2016.
- [34] Ernst Hairer and Gerhard Wanner. *Solving ordinary differential equations II: Stiff and differential-algebraic problems*. Springer Berlin Heidelberg, 1996.
- [35] Will Pazner and Per-Olof Persson. Stage-parallel fully implicit Runge–Kutta solvers for discontinuous Galerkin fluid simulations. *Journal of Computational Physics*, 335:700 – 717, 2017.
- [36] Anders C. Hansen and John Strain. On the order of deferred correction. *Applied Numerical Mathematics*, 61(8):961–973, August 2011.
- [37] Tao Tang, Hehu Xie, and Xiaobo Yin. High-order convergence of spectral deferred correction methods on general quadrature nodes. *Journal of Scientific Computing*, 56(1):1–13, October 2012.

- [38] Roberto Bagnara. A unified proof for the convergence of jacobi and gauss–seidel methods. *SIAM review*, 37(1):93–97, 1995.
- [39] TE Tezduyar and YJ Park. Discontinuity-capturing finite element formulations for nonlinear convection-diffusion-reaction equations. *Computer Methods in Applied Mechanics and Engineering*, 59(3):307–325, 1986.
- [40] Donald J Estep, Mats G Larson, and Roy D Williams. *Estimating the error of numerical solutions of systems of reaction-diffusion equations*, volume 696. American Mathematical Society, 2000.
- [41] Donald J Estep and Roland W Freund. Using Krylov-subspace iterations in discontinuous Galerkin methods for nonlinear reaction-diffusion systems. In *Discontinuous Galerkin Methods*, pages 327–335. Springer, 2000.
- [42] Jaime Peraire and P-O Persson. The compact discontinuous Galerkin (CDG) method for elliptic problems. *SIAM Journal on Scientific Computing*, 30(4):1806–1824, 2008.
- [43] Wolfgang A Wall. *Fluid-struktur-interaktion mit stabilisierten finiten elementen*. Institut für Baustatik der Universität Stuttgart, 1999.
- [44] Christiane Förster, Wolfgang A Wall, and Ekkehard Ramm. Artificial added mass instabilities in sequential staggered coupling of nonlinear structures and incompressible viscous flows. *Computer Methods in Applied Mechanics and Engineering*, 196(7):1278–1293, 2007.
- [45] Jean-Frédéric Gerbeau and Marina Vidrascu. A quasi-newton algorithm based on a reduced model for fluid-structure interaction problems in blood flows. *ESAIM: Mathematical Modelling and Numerical Analysis*, 37(4):631–647, 2003.
- [46] Christophe Kassiotis, Adnan Ibrahimbegovic, Rainer Niekamp, and Hermann G Matthies. Nonlinear fluid-structure interaction problem. part i: implicit partitioned algorithm, nonlinear stability proof and validation examples. *Computational Mechanics*, 47(3):305–323, 2011.
- [47] Charbel Habchi, Serge Russeil, Daniel Bougeard, Jean-Luc Harion, Thierry Lemenand, Akram Ghanem, Dominique Della Valle, and Hassan Peerhossaini. Partitioned solver for strongly coupled fluid-structure interaction. *Computers & Fluids*, 71:306–319, 2013.
- [48] Ulrich Küttler, Christiane Förster, and Wolfgang A Wall. A solution for the incompressibility dilemma in partitioned fluid-structure interaction with pure dirichlet fluid domains. *Computational Mechanics*, 38(4-5):417–429, 2006.
- [49] Ch Förster, Wolfgang A Wall, and Ekkehard Ramm. On the geometric conservation law in transient flow calculations on deforming domains. *International Journal for Numerical Methods in Fluids*, 50(12):1369–1379, 2006.
- [50] Jean Donea and Antonio Huerta. *Finite element methods for flow problems*. John Wiley & Sons, 2003.
- [51] EH Van Brummelen. Added mass effects of compressible and incompressible flows in fluid-structure interaction. *Journal of Applied mechanics*, 76(2):021206, 2009.
- [52] René De Borst, Mike A Crisfield, Joris JC Remmers, and Clemens V Verhoosel. *Nonlinear finite element analysis of solids and structures*. John Wiley & Sons, 2012.
- [53] Charbel Farhat, Michel Lesoinne, and Nathan Maman. Mixed explicit/implicit time integration of coupled aeroelastic problems: Three-field formulation, geometric conservation and distributed solution. *International Journal for Numerical Methods in Fluids*, 21(10):807–835, 1995.
- [54] Ch Farhat, C Degand, B Koobus, and M Lesoinne. Torsional springs for two-dimensional dynamic unstructured fluid meshes. *Computer Methods in Applied Mechanics and Engineering*, 163(1-4):231–245, 1998.
- [55] Charbel Farhat, Michael Lesoinne, and Patrick Le Tallec. Load and motion transfer algorithms for fluid/structure interaction problems with non-matching discrete interfaces: Momentum and energy conservation, optimal discretization and application to aeroelasticity. *Computer Methods in Applied Mechanics and Engineering*, 157(1-2):95–114, 1998.

- [56] Jintai Chung and GM Hulbert. A time integration algorithm for structural dynamics with improved numerical dissipation: the generalized- α method. *Journal of applied mechanics*, 60(2):371–375, 1993.
- [57] Zhangli Peng and Qiang Zhu. Energy harvesting through flow-induced oscillations of a foil. *Physics of Fluids*, 21(12):123602, 2009.
- [58] Matthew J Zahr and P-O Persson. An adjoint method for a high-order discretization of deforming domain conservation laws for optimization of flow problems. *Journal of Computational Physics*, 326:516–543, 2016.
- [59] P-O Persson, J Bonet, and J Peraire. Discontinuous Galerkin solution of the Navier–Stokes equations on deformable domains. *Computer Methods in Applied Mechanics and Engineering*, 198(17-20):1585–1595, 2009.
- [60] Philip L Roe. Approximate Riemann solvers, parameter vectors, and difference schemes. *Journal of Computational Physics*, 43(2):357–372, 1981.
- [61] Chi-Kun Lin. On the incompressible limit of the compressible Navier-Stokes equations. *Communications in Partial Differential Equations*, 20(3-4):677–707, 1995.
- [62] Benoît Desjardins, Emmanuel Grenier, P-L Lions, and Nader Masmoudi. Incompressible limit for solutions of the isentropic Navier-Stokes equations with Dirichlet boundary conditions. *Journal de Mathématiques Pures et Appliquées*, 78(5):461–471, 1999.
- [63] Matthew Emmett and Michael Minion. Toward an efficient parallel in time method for partial differential equations. *Communications in Applied Mathematics and Computational Science*, 7(1):105–132, March 2012.